RAPID COMMUNICATIONS IN MASS SPECTROMETRY
Rapid Commun. Mass Spectrom. 2010; **24**: 2999–3010
Published online in Wiley Online Library (wileyonlinelibrary.com) DOI: 10.1002/rcm.4722

RCM

Elucidation of the decomposition pathways of protonated and deprotonated estrone ions: application to the identification of photolysis products

Sophie Bourcier*, Clémentine Poisson, Yasmine Souissi, Said Kinani, Stéphane Bouchonnet and Michel Sablier

Ecole Polytechnique et CNRS, Département de Chimie, Laboratoire des Mécanismes Réactionnels (DCMR), UMR 7651, 91128 Palaiseau Cedex, France

Received 18 June 2010; Revised 22 July 2010; Accepted 22 July 2010

With the future aim of elucidating the unknown structures of estrogen degradation products, we characterized the dissociation pathways of protonated estrone (E1) under collisional activation in liquid chromatography/tandem mass spectrometry (LC/MS/MS) experiments employing a quadrupole time-of-flight mass spectrometer. Positive ion and negative ion modes give information on the protonated and deprotonated molecules and their product ions. The mass spectra of estrone methyl ether (CH_3-E1) and estrone-d_4 (E1-d_4) were compared with that of E1 in order (i) to elucidate the dissociation mechanisms of protonated and deprotonated molecules and (ii) to propose likely structures for each product ions. The positive ion acquisition mode yielded more fragmentation. The mass spectra of E1 were compared with those of estradiol (E2), estriol (E3) and 17-ethynylestradiol (EE2). This comparison allowed the identification of marker ions for each ring of the estrogenic structure. Accurate mass measurements have been carried out for all the identified ions. The resulting ions revealed to be useful for the characterization of structural modifications induced by photolysis on each ring of the estrone molecule. These results are very promising for the determination of new metabolites in the environment. Copyright © 2010 John Wiley & Sons, Ltd.

Endocrine-disrupting chemicals (EDCs) have become a major public health concern because of their detrimental effects on the human and animal endocrine system.[1–3] EDCs have the ability to alter or disrupt normal hormonal functions mimicking the behaviour of estrogen and androgen steroid hormones. EDCs in the environment and food have various origins; the main source has been attributed to human activity via discharge of industrial waste, municipal sewage, urban and agricultural runoff. Photo-transformation reactions are currently suggested to play an important role in the elimination of pollutants from surface waters,[4] and ultraviolet (UV) light irradiation is an established method for drinking-water disinfection and wastewater purification. Among the wide range of EDCs encountered in the environment, endogenous estrogens such as 17β-estradiol (E2) and estrone (E1) are of particular concern due to their high physiologic activity; they exert estrogenic effects in fish at low levels.[5] Moreover, estrogens present molecular features that make them liable to photodecomposition under solar light.[6] The effect of the presence of EDCs in the environment still remains largely unknown; some pessimistic impacts in a large number of species ranging from invertebrates to humans have been reported in numerous comprehensive studies. These chemicals have been demonstrated to cause significant ecotoxicological effects such as sex ratio changes, reduction of fecundity and fertilization rate on fish and other wildlife.[7] Consequently, developing highly sensitive and practical analytical methods to detect and quantify EDCs in environmental (water, soil, sediments...) and biological (animals and plants) matrices has become a challenge in environmental science research. Two approaches are known to be very sensitive for the screening of these compounds. The first approach consists of detecting EDCs using physicochemical methods, especially high-performance liquid chromatography and gas chromatography coupled with mass spectrometry (LC/MS[8,9] and GC/MS[10]). Recent studies have demonstrated the potential of using LC/MS electrospray ionization in the negative ion mode for the detection of estrogens.[11,12] The second approach consists of measuring the biological activity exerted by EDCs using bioanalytical methods, especially *in vitro* and *in vivo* bioassays.[13] Recently, we carried out a study on river sediments with the aim of establishing a reliable correlation between the nature of the endocrine disruption observed and the EDCs dectected.[14] This approach, referred to as ''effect directed analysis'', consisted of fractioning sediment extracts by preparative chromatography and submitting each collected fraction to chemical analysis and bioassays. The main result of this work consisted of demonstrating that some fractions induced an

*Correspondence to: S. Bourcier, Ecole Polytechnique et CNRS, Département de Chimie, Laboratoire des Mécanismes Réactionnels (DCMR), UMR 7651, 91128 Palaiseau Cedex, France.
E-mail: sophie.bourcier@dcmr.polytechnique.fr

intense estrogenic activity although they did not contain any of the targeted EDCs. Therefore, attention was focused on the need to identify degradation products of these estrogens since they are suspected to be responsible for the estrogenic activity measured. Usually, characterization of such compounds in environmental matrices requires the use of particular MS methods such as neutral loss scanning or product ion scan.[15] Further development of efficient MS methods would enable us to determine if specific marker ions of the compounds of interest could be used to characterize the scrutinized species. Several studies devoted to the identification of photoproducts of estrogenic compounds have been carried out in recent years.[16–18] Some of them used tandem mass spectrometry (MS/MS) modes such as precursor ion scanning to show evidence for the presence of several compounds of a given family. However, due to the complexity of photolysis reactions, dissociation pathways were not elucidated making the determination of photoproduct chemical structures difficult. In the work of Mazellier *et al.* the chemical structures of degradation products are deduced from molecular weights.[19] To our knowledge, the use of marker ions observed under LC/MS/MS conditions has not been previously reported for the identification of photoproducts of estrogenic compounds. With the future aim of elucidating the unknown structures of the degradation products of estrone (E1), we characterized the dissociation pathways of protonated estrone under collisional activation in LC/MS/MS experiments employing a quadrupole time-of-flight mass spectrometer. Electrospray ionization of analytes was performed in both positive and negative ion modes. The mass spectra of estrone methyl ether (CH_3-E1) and estrone-d_4 (E1-d_4) were compared with that of E1 in order (i) to elucidate the dissociation mechanisms of the protonated and deprotonated molecules and (ii) to propose likely structures for each product ion. The mass spectra of E1 were compared with those of estradiol (E2), estriol (E3) and 17-ethynilestradiol (EE2). This comparison allowed marker ions to be identified for each ring of the estrogenic structure. Accurate mass measurements have been carried out for all the identified ions. The last part of this work shows how the chemical structure of a photolysis product of estrone was elucidated based on knowledge of the fragmentation pathways, thus illustrating the value of this type of mechanistic study.

EXPERIMENTAL

Chemicals and reagents

The chemical structures of estrone (E1, R = X = X′ = Y = Y′ = H, compound **1**), estrone methyl ether (CH_3-E1, R = CH_3, X = X′ = Y = Y′ = H, compound **2**), estrone-d_4 (E1-d_4, R = H, X = X′ = Y = Y′ = D, compound **3**), estradiol (E2), estriol (E3) and 17-ethynylestradiol (EE2) are displayed in Table 1. Chemicals, formic acid and HPLC grade solvents were all purchased from Sigma Aldrich (Saint Quentin Fallavier, France) and used as received.

Standard solutions

Solutions of each compound at 10^{-2} M were prepared in methanol and stored at −20°C. These solutions were diluted to 10^{-6} M in a H_2O/CH_3CN (50:50) mixture for the acquisition of mass spectra in the negative ion mode. The same mixture was acidified with formic acid (0.1%) for acquisitions in the positive ion mode. For photolytic experiments, a stock solution of estrone was prepared by dissolving the hormone in ultra-pure water under sonication at a concentration of 0.25 mg.mL^{-1}.

Procedure for photolytic experiments

Photolysis experiments were carried out in a 250 mL quartz cylindrical reactor equipped with a high-pressure mercury lamp (HPL-N 125W/542 E27 SG; Philips, Ivry sur Seine, France) with an emission band extending from 250 to 620 nm. The lamp was placed into the inner part of the reactor cooled by water circulation to avoid uncontrolled heating of the irradiated solution in maintaining a constant temperature of 25 ± 2°C. The luminous flux emitted from the HPL-N lamp was reported by the manufacturer to be 6200 lm. The solution was stirred during radiation time with a sonicator (Bioblock Scientific, Illkirch, France). The photoreactor was filled with 30 mL of stock solutions and irradiated by the mercury lamp for 90 min. The reactor was wrapped up by an aluminum foil to optimize UV-visible irradiation of the solution, and to avoid emission outside the reactor. Afterwards, the irradiated solution was recovered and concentrated using a rotavapor set-up (Büchi, Rungis, France). The dry residue was subsequently rediluted in 7 mL of methanol and then dried under a nitrogen flow. Then 1 mL of methanol was added to the dry extract and 100 μL of this solution were evaporated to dryness under a nitrogen flow and diluted with 200 μL of an acidified solution (0.1% formic acid) of H_2O/CH_3CN (60:40).

Mass spectrometric conditions

Electrospray ionization (ESI) – apparatus and parameters

ESI-MS/MS analyses were carried out with a quadrupole time-of flight mass spectrometer (Q-TOF Premier) equipped with a Z-spray electrospray source (Waters, Saint Quentin-en-Yvelines, France). Two acquisition modes were used to characterize each compound: (i) full scan mode and (ii) MS/MS of the precursor ion. For fragmentation studies, solutions were infused into the ESI source with a syringe pump at an infusion rate of 10 μL.min^{-1}. For the study of photolysis degradation products, the sample was analyzed using a 2690 liquid chromatography module from Waters coupled with the Q-TOF Premier mass spectrometer. The analytical column used was a Pursuit XRs Ultra 2.8 C18 (50 × 2.0 mm; Varian, Les Ulis, France). The HPLC solvents were acetonitrile with 0.1% formic acid (A) and water with 0.1% formic acid (B). The following program of linear gradient elution was applied: 40% of A for 11 min and 40–100% of A from 11.1 to 20 min. The column was reconditioned with 40% of A for 10 min between two injections. The effluent was introduced at a rate of 0.2 mL.min^{-1} into the Z-spray interface for ionization.

The full scan acquisition mode allowed the optimization of the cone voltage to obtain the maximum precursor ion intensity. Several MS/MS spectra were recorded to study

DOI: 10.1002/rcm

Table 1. Names and chemical structures of the studied compounds

	Compound	Code	MW	Structure
				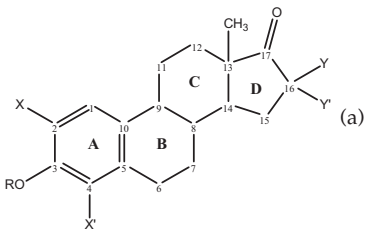 (a)
1	Estrone	E1	270	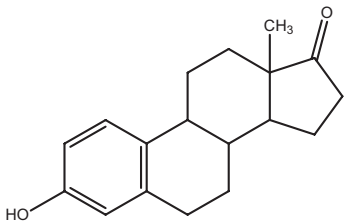
2	Estrone methyl ether	CH_3-E1	284	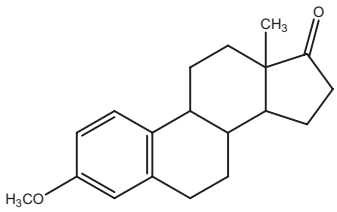
3	Estrone-d_4	E1-d_4	274	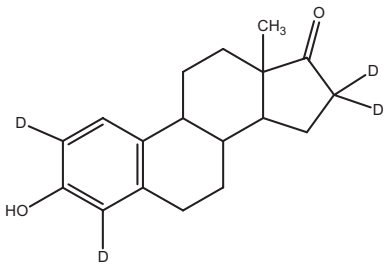
	17α-Estradiol	E2	272	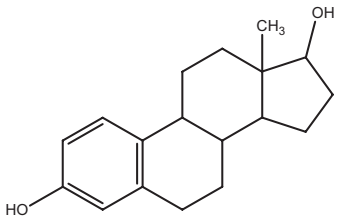
	Estriol	E3	288	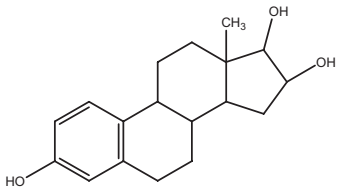
	17α-Ethynylestradiol	EE2	296	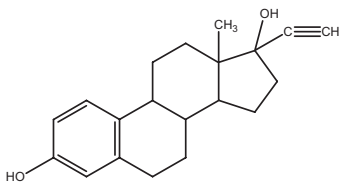

(a) See Experimental section for definitions of R, X, X′, Y and Y′.

DOI: 10.1002/rcm

RCM

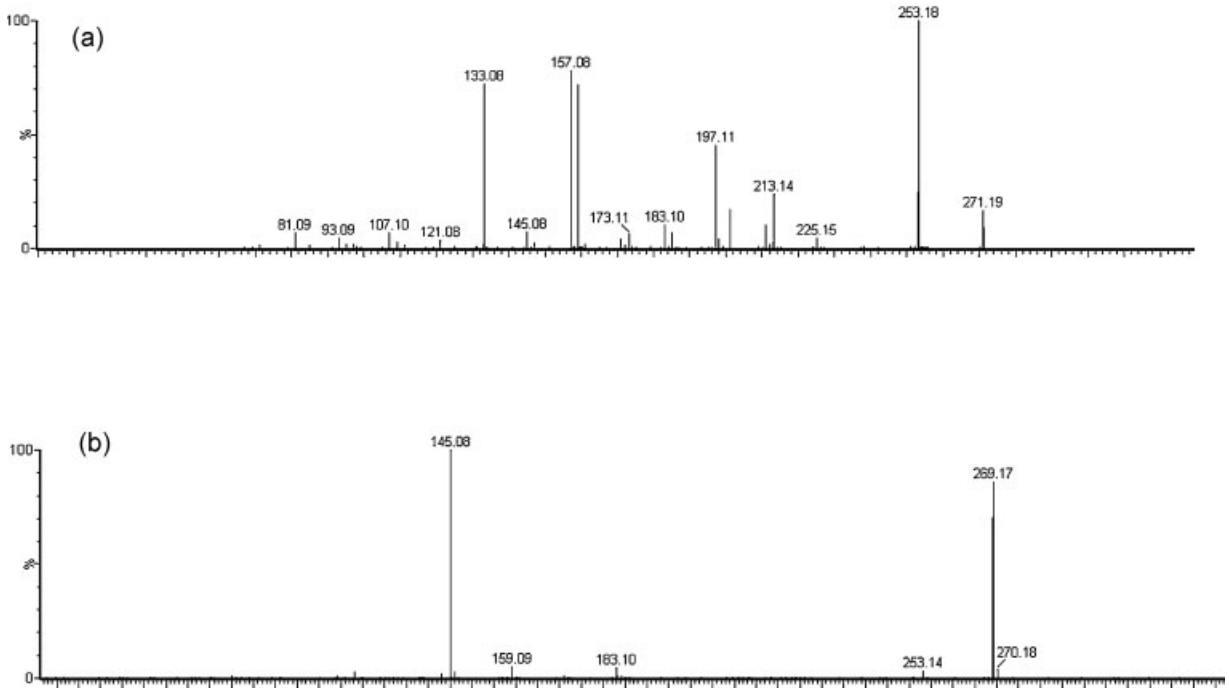

Figure 1. CID mass spectra of protonated and deprotonated estrone: (a) $[\mathbf{1}H]^+$ recorded with a collision energy of 15 eV and (b) $[\mathbf{1}–H]^-$ recorded with a collision energy of 25 eV. The cone voltage was set at 30 V in both cases.

decomposition pathways. The decomposition of ions of interest was studied as a function of the collision energy in the laboratory frame (E_{lab}), typically in the 0–30 eV range. The results are presented in Fig. 2. The cone voltage was adjusted for each ion of interest generated in the ion source. The ion signals were optimized by adjusting the source parameters as follows: the cone voltage was set between 20 and 80 V while the capillary voltage was set to 3.2 kV and −3.2 kV for positive ion and negative ion mode, respectively. Typical values for the other source parameters were an extraction cone voltage of 2 V and an ion guide voltage of 2.4 V. The source and desolvation temperatures were set at 80°C and 120°C, respectively, for direct infusion and at 120°C and 450°C, respectively, for LC/MS studies. Nitrogen was used as both nebulizing and desolvation

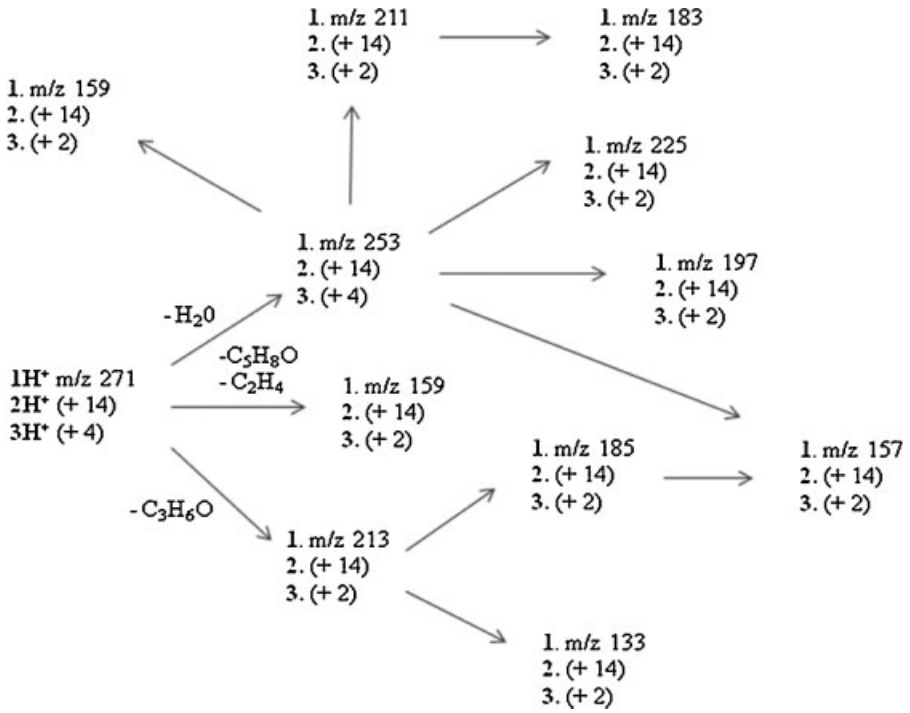

Figure 2. Decomposition pathways of MH^+ ions of E1 (**1**, *m/z* 271) observed by MS/MS experiments. *m/z* shifts observed for the corresponding ions in the CID mass spectra of CH_3-E1 (**2**, *m/z* 285) and E1-d_4 (**3**, *m/z* 275) are given in parentheses.

DOI: 10.1002/rcm

gas. The gas flows were dependent on the introduction mode, ranging from 20 to 300 L.h^{-1} for direct introduction and from 70 to 700 L.h^{-1} for LC/MS. For LC/MS analysis, the volume injected was 10 μL. Argon was used as the collision gas at a flow of 0.26 mL.min^{-1}, corresponding to a pressure of 2 10^{-3} mbar. Accurate mass measurements were acquired using an independent reference spray via the LockSpray interface to ensure accuracy. Phosphoric acid, at a flow rate of 10 μLmin^{-1}, was used (in positive and negative ion mode) to provide the lock mass. The LockSray frequency was set at 10 s and data for the reference compounds were averaged over 10 spectra min^{-1}. The accurate mass and the elemental composition for all ions were obtained using the instrument MassLynx software. The ions used for the mass correction were *m/z* 294.9685 and 292.9229 for ions with *m/z* values above 200 and *m/z* 196.9616 and 194.946 for the others in positive and negative ion mode, respectively.

RESULTS AND DISCUSSION

Fragmentation pathways

Figure 1 displays the collision-induced dissociation (CID) mass spectra of protonated (MH^+) and deprotonated ($[M-H]^-$) estrone recorded using collision energies of 15 and 25 eV in positive and negative ion mode, respectively. These collision energies reflected the best fragmentation conditions of the precursor ions. It has been reported that the negative ion mode is preferred for the identification of target estrogens in biological matrices.[20,21] In this work, the $[M-H]^-$ ion dissociates to provide a major product ion at *m/z* 145, while CID of the MH^+ ions leads to the formation of several product ions. Table 2 lists the product ions obtained under CID of the MH^+ and $[M-H]^-$ ions of E1, E2, E3 and EE2 in positive ion (ESI-P) and negative ion mode (ESI-N). Figure 2 shows the MS/MS transitions established by experiments for E1, CH_3-E1 and E1-d_4. The shifts in *m/z* values observed for each ion, relative to the corresponding E1 ion, are given in parentheses. We compared the behavior of the three compounds under CID to propose fragmentation mechanisms and to deduce the chemical structures of product ions. The accurate mass measurements of all estrone ions are listed in Table 3.

Table 2. Main product ions from the CID mass spectra of MH^+ and $[M-H]^-$ ions of estrogenic compounds obtained in positive ion (ESI-P) and negative ion (ESI-N) acquisition modes

Compounds	ESI-P								ESI-N
m/z	133	157	159	183	185	197	213	$[MH-H_2O]^+$	145
E1	+	+	+	+	+	+	+	+	+
E2	+	−	+	+	−	−	−	+	+
E3	+	+	+	+	−	+	+	+	+
EE2	+	−	+	+	−	−	−	+	+

(+) detected; (−) non detected.

Table 3. Accurate mass measurements of estrone ions obtained in a standard solution

Ions *m/z*	Elemental composition	Experimental mass (*m/z*)	Theorical mass (*m/z*)	mDa	Error (ppm)	DBE[a]	Scheme[b]
ESI-N							
269	$C_{18}H_{21}O_2$	269.1546	269.1542	0.4	1.5	8.5	1
145	$C_{10}H_9O$	145.0646	145.0653	−0.7	−4.8	6.5	1
ESI-P							
271	$C_{18}H_{23}O_2$	271.1693	271.1698	−0.5	−1.8	7.5	2 - 3 - 4
253	$C_{18}H_{21}O$	253.1592	253.1592	0	0	8.5	2
225	$C_{16}H_{17}O$	225.1276	225.1279	−0.3	−1.3	8.5	2
213	$C_{15}H_{17}O$	213.1268	213.1279	−1.1	−5.2	7.5	3
211	$C_{15}H_{15}O$	211.1123	211.1123	0	0	8.5	2
197	$C_{14}H_{13}O$	197.0959	197.0966	−0.7	−3.6	8.5	2
185	$C_{13}H_{13}O$	185.0960	185.0966	−0.6	−3.2	7.5	3
183	$C_{13}H_{11}O$	183.0817	183.0810	−0.7	−3.8	8.5	2
159	$C_{11}H_{11}O$	159.0815	159.0810	0.5	3.1	6.5	2 - 4
157	$C_{11}H_9O$	157.0659	157.0653	0.6	3.8	7.5	3
133	C_9H_9O	133.0654	133.0653	0.1	0.8	5.5	3

[a] DBE: Double-bond equivalency.
[b] Number of the scheme in which the ion structure is displayed.

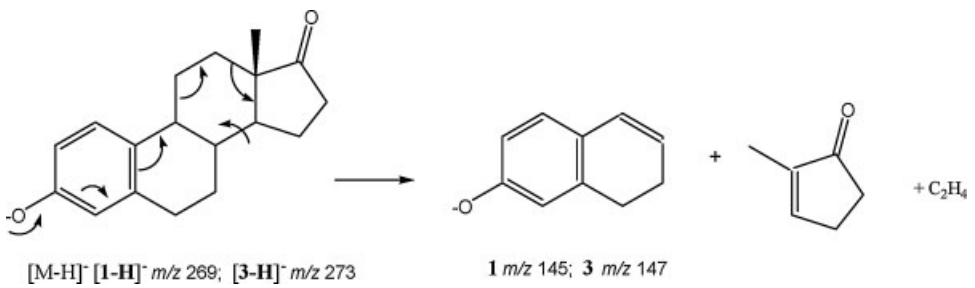

Scheme 1. Decomposition of the $[M-H]^-$ ion of estrone.

DOI: 10.1002/rcm

RCM

Decomposition of $[M-H]^-$ ions

CID experiments on the $[M-H]^-$ ions of E1 lead to only one product ion of significant abundance at *m/z* 145 (shifted to *m/z* 147 for E1-d_4). This ion is common to all the estrogenic compounds studied (see Table 2) and could thus be used as a marker ion to detect molecules belonging to the same family using a precursor ion scan mode procedure. Formation of the *m/z* 145 ion from $[M-H]^-$ is assumed to result from a charge-remote concerted mechanism after deprotonation of the hydroxyl function of the phenol group (Scheme 1). The structure proposed for the *m/z* 145 ion is in agreement with the shift to *m/z* 147 observed in the E1-d_4 mass spectrum.

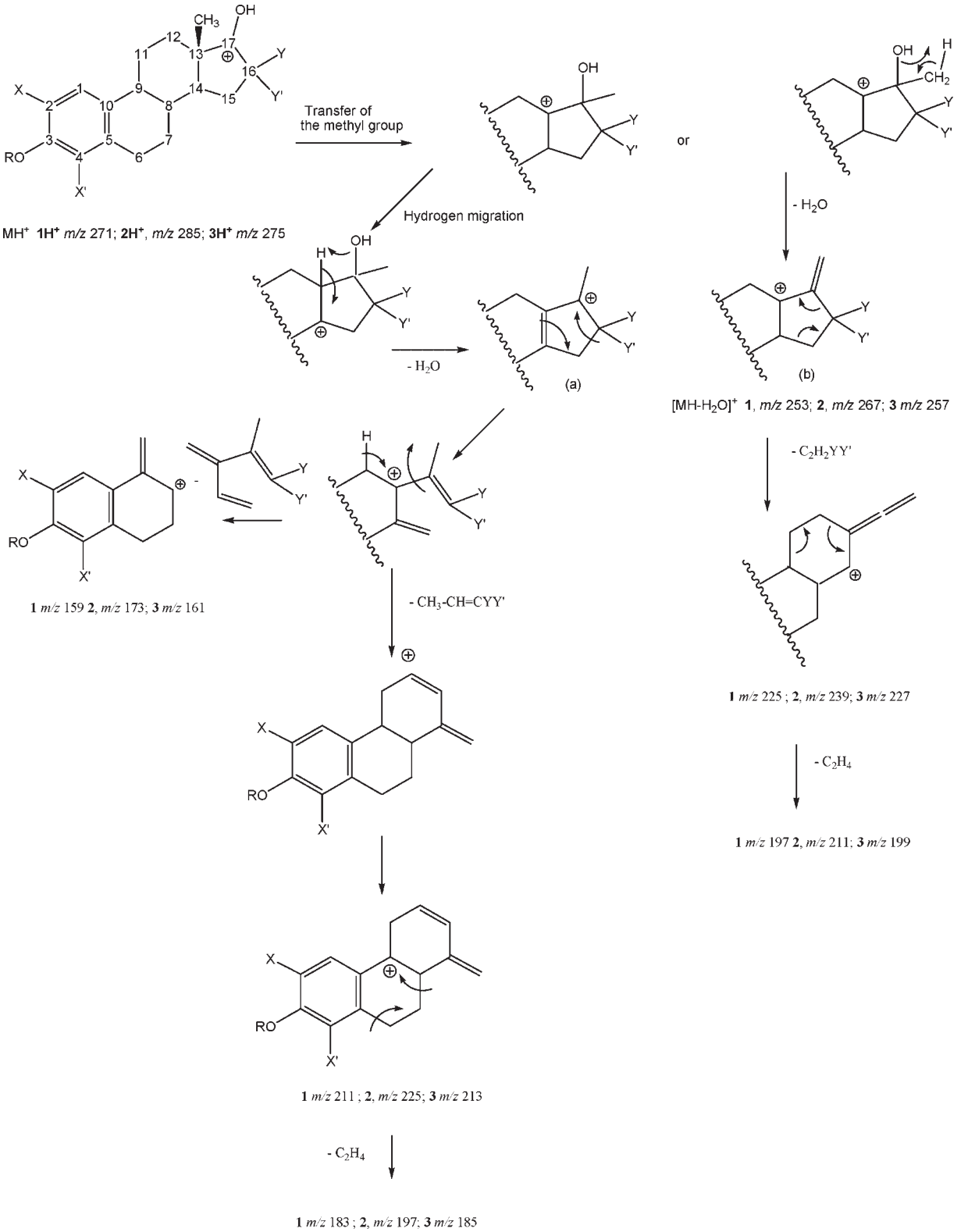

Scheme 2. Loss of water from MH^+ ions and subsequent fragmentations.

DOI: 10.1002/rcm

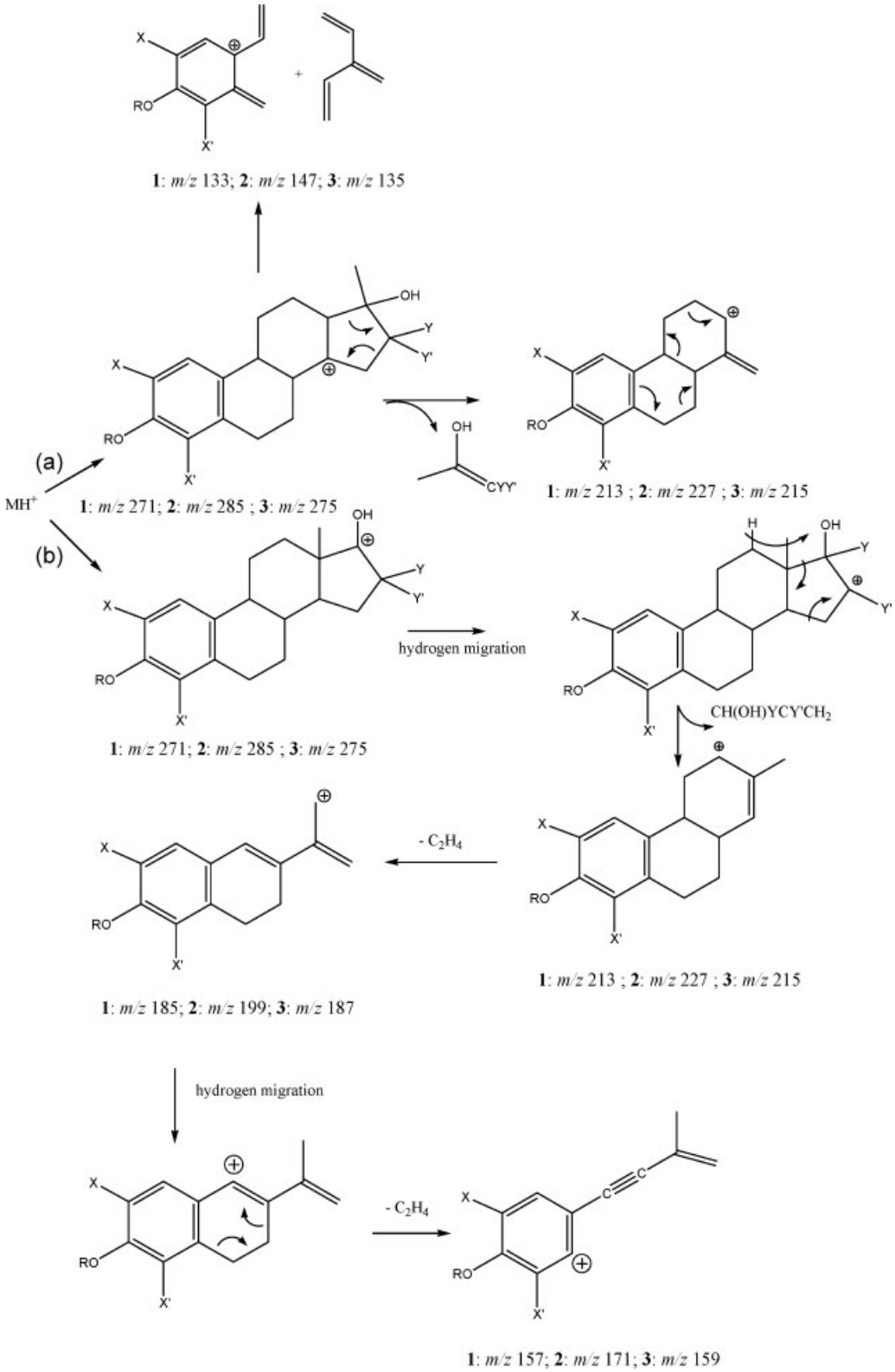

Scheme 3. Mechanism of formation and decomposition of the *m/z* 213 ion from $[\mathbf{1}H]^+$.

Decomposition of $[MH]^+$ ions

The main product ions of MH^+ were identified by MS/MS experiments performed with collision energies ranging from 2 to 30 eV. The transitions are summarized in Fig. 2. $[\mathbf{1}H]^+$ ions undergo either (i) loss of water leading to the *m/z* 253 ion, (ii) loss of C_3H_6O leading to the *m/z* 213 ion, or (iii) loss of $C_7H_{10}OYY'$ leading to the *m/z* 159 ion.

Water elimination

The water loss also observed in the dissociation pathways of protonated estrone methyl ether ($\mathbf{2}H^+$) (*m/z* 285 → 267) should result from protonation on the oxygen atom of the ketone, ring D. The lack of DOH elimination in the dissociation pathways of deuterated E1-d_4 ($\mathbf{3}H^+$) demonstrates that the hydrogen atoms at the C16 position (see

DOI: 10.1002/rcm

Table 1 for numbering of the carbon atoms) are not involved in the water elimination process. The mechanism proposed to explain the formation of $[MH-H_2O]^+$ implies a transfer of the methyl group from C13 to C17, as presented in the upper part of Scheme 2. Such a 1,2-transfer of a methyl anion to an adjacent positively charged carbon atom has been previously reported.[22] The second hydrogen atom of the eliminated water molecule could come either from the methyl group on C17, through a four-center concerted mechanism leading to the ion (b) in Scheme 2, or from the C14 position after the migration of a hydrogen atom from C14 to C13 via a four-center concerted mechanism, leading to the ion (a) in Scheme 2. In both cases, the elimination of water leads to a tertiary stable carbocation conjugated with a carbon–carbon double bond.

Mechanisms of formation of the ions at *m/z* 211 and 183 from the $[\mathbf{1}H-H_2O]^+$ ion are proposed on the right-hand side of Scheme 2. The formation of the *m/z* 211 ion implies the loss of $(CH_3)CH=CH_2$ from structure (a) of ion $[\mathbf{1}H-H_2O]^+$. The formation of *m/z* 183 from *m/z* 211 implies the loss of C_2H_4. The *m/z* 211 ions are shifted to *m/z* 225 and 213 in the CID mass spectra of CH_3-E1 ($\mathbf{2}H^+$) and E1-d_4 ($\mathbf{3}H^+$), respectively, indicating that the aromatic ring A substituted with the hydroxyl group remains unchanged in the *m/z* 211 ion structure. The formation of *m/z* 159 from *m/z* 253 (structure (a)) could be explained by elimination of C_7H_{10}. The mechanism of formation of the ions at *m/z* 225 and 197 from the $[\mathbf{1}H-H_2O]^+$ ion structure (b) involves two successive losses of ethene. The *m/z* 225 ion is shifted to *m/z* 239 and 227 in the CID mass spectra of CH_3-E1 ($\mathbf{2}H^+$) and E1-d_4 ($\mathbf{3}H^+$), respectively, in agreement with the elimination of C_2H_2YY'.

$C_3H_4YY'O$ elimination

The $\mathbf{1}H^+$ decomposition pathways leading to *m/z* 213 are displayed in Scheme 3. Two pathways could lead to the formation of *m/z* 213 from $\mathbf{1}H^+$. The first one (pathway (a)) is from the $\mathbf{1}H^+$ ion obtained by hydride transfer from C14 to C13 after migration of the methyl group from C13 to C17. In this case, the elimination of 2-hydroxypropene $(CH_3)C(OH)=CH_2$ via a concerted mechanism leads directly to the formation of the *m/z* 213 ion. The second one (pathway (b)) is from the $\mathbf{1}H^+$ ion after migration of a hydrogen atom Y from C16 to C17, this ion loses $CH(OH)YCY'CH_2$ after migration of a hydrogen atom from C12 to C17. As for the decomposition of *m/z* 253, *m/z* 213 can lose one or two ethene molecules to yield the ions at *m/z* 185 and 157. The formation of *m/z* 133 can be rationalized by a concerted mechanism leading to the elimination of a C_6H_8 molecule from the *m/z* 213 ion.

$C_7H_{10}OYY'$ elimination

The formation of the *m/z* 159 ion results from elimination of $C_7H_{10}OYY'$ from $\mathbf{1}H^+$ protonated on the oxygen atom of the ketone function and after migration of a methyl group (Scheme 4).

In summary, the five ions at *m/z* 133, 157, 159, 197 and 253 observed in the CID mass spectrum of $\mathbf{1}H^+$ with relatively high abundance (Fig. 1) have preserved the hydroxyl-substituted aromatic ring A. Thus, the three ions, *m/z* 133, 157 and 159, can be considered as characteristic of ring A of the steroidal structure, while the *m/z* 197 ion gives information on the substitution of the B and C rings through the subsequent ethene eliminations in ($\mathbf{1}H^+$) (Scheme 2, right side). Only the MH^+ and $[MH-H_2O]^+$ ions provide information about substitution on the D ring since the substituents Y and Y' on the C16 carbon atom still remain after water loss. The high resolving power provided by the TOF instruments allowed us to obtain accurate mass measurements (see Table 3). The structures proposed in the fragmentation schemes are in agreement with the elemental compositions of the precursor and characteristic product ions. The errors were mostly lower than 5 ppm and, therefore, offer a high degree of confidence in the proposed structures.

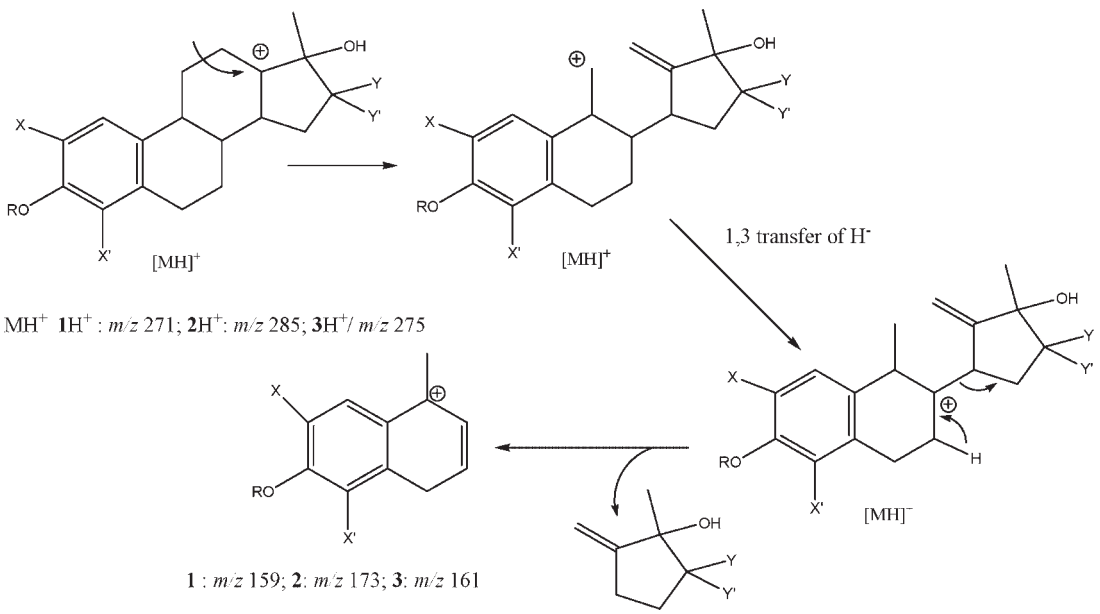

Scheme 4. Mechanism of formation of the *m/z* 159 ion from $[\mathbf{1}H]^+$.

DOI: 10.1002/rcm

Characteristic ions in the CID mass spectra of estrogenic compounds

Table 2 summarizes the CID mass spectra of the MH^+ and $[M-H]^-$ ions of the estrogens studied. In positive ion mode, four ions at *m/z* 133, 159, 183, $[MH-H_2O]^+$ and the protonated molecule MH^+ are observed for all analytes, while only two ions, *m/z* 145 and $[M-H]^-$, are observed in the negative ion mode. From these data, it can be concluded that the positive acquisition mode should be more useful for the characterization of photodegradation products since the four product ions detected in addition to the MH^+ ion allow the A, B, C and D rings of the steroid to be characterized. This point will be demonstrated in the following part of the paper.

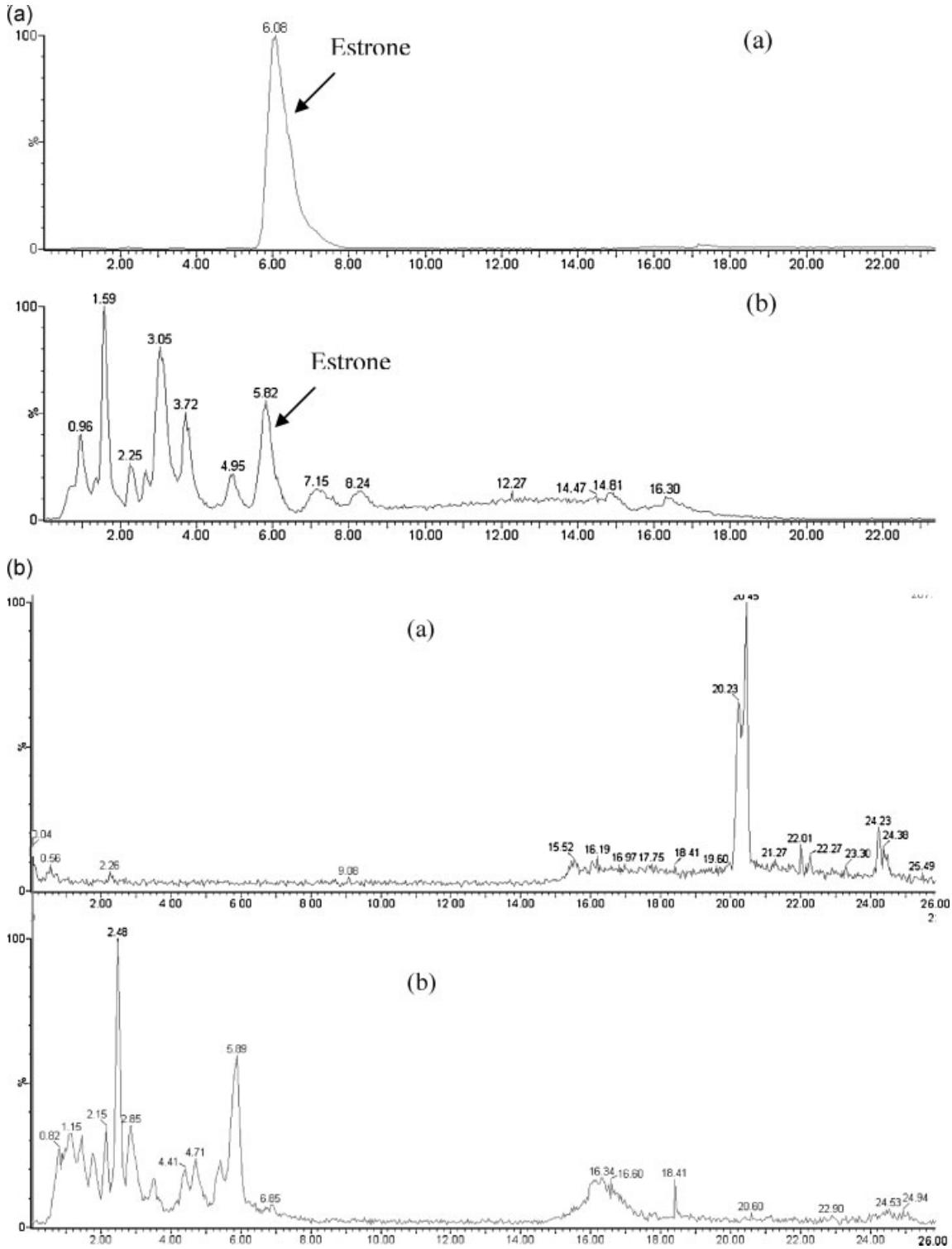

Figure 3. (a) Extracted ion chromatograms of *m/z* 271 $[MH]^+$ and *m/z* 253 $[MH-H_2O]^+$ for (a) reference estrone solution and (b) irradiated estrone solution. (b) Extracted ion chromatograms of *m/z* 287 $[M_{ox}H]^+$ and *m/z* 269 $[M_{ox}H\text{-}H_2O]^+$ for (a) reference estrone solution and (b) irradiated estrone solution.

DOI: 10.1002/rcm

Structural characterization of photodegradation products of estrone

The information obtained from the CID study of protonated estrone has been applied to the identification of photodegradation products. An example is described here to illustrate how a detailed description of the fragmentation mechanisms of the protonated molecules of E1 provides structural information on the degradation compounds of E1. The photolysis of estrone was performed as described in the Experimental section. The identification of the photodegradation products includes two experimental steps. The first consists of recording full scan mass spectra at low cone voltage and low collision energy to preserve the protonated molecule structures for both the irradiated and the reference estrone solutions. The resulting chromatograms for the two solutions are then compared (see Figs. 3(a) and 3(b)). After the identification of $[M+H]^+$ ions from new molecules in the irradiated solution, the second part of the work consists of the identification of these compounds on the basis of their CID mass spectra recorded with the parameters optimized for estrone. Several photodegradation products were observed. As described previously,[19,23] photolysis of estrone steroids leads preferentially to the formation of oxidation compounds. We therefore searched in the chromatograms for $[MH+16]^+$ ions at *m/z* 287, corresponding to protonated oxidized estrone. We assume that these ions can lose a water molecule to give $[M_{ox}H-H_2O]^+$ ions at *m/z* 269. Figures 3(a) and 3(b) show the extracted ion currents for *m/z* 271 $(\mathbf{1}H^+)$ + *m/z* 253 $(\mathbf{1}H-H_2O)^+$ (Fig. 3(a)), and for *m/z* 287 + *m/z* 269, corresponding to the ions of oxidized compounds (Fig. 3(b)) for the reference solution of estrone on chromatograms (a) and for the irradiated estrone solution on chromatograms (b). These results show that the irradiation of estrone leads to the formation of photoproducts corresponding to (i) isomers of protonated estrone (see Fig. 3(a), chromatogram (b)), and (ii) oxidized compounds (see Fig. 3(b), chromatogram (b)). To exemplify our approach, we focused on the identification of the oxidized compound eluted at a retention time of 2.48 min.

Figure 4 shows a comparison of the CID mass spectra of the MH^+ ion of estrone and of the $M_{ox}H^+$ ion for the irradiated solution. The CID mass spectrum of $M_{ox}H^+$ shows (i) ions at the same *m/z* values as those obtained in the spectrum of $(\mathbf{1}H^+)$: *m/z* 133; 157; 159; and 173 with different relative intensities, and (ii) other ions shifted to 16 *m/z* units higher: *m/z* 173 (*m/z* 157 + 16), 213 (*m/z* 197 + 16); 227; (*m/z* 211 + 16); 269 (*m/z* 253 + 16); and 287 (*m/z* 271 + 16), corresponding to ions that included a supplementary oxygen atom (See Fig. 4). To localize the ring where the oxidation has taken place, we have compared in Fig. 5 the CID mass spectrum of $[\mathbf{1}H-H_2O]^+$ (spectrum (a)) with that of $[M_{ox}H-H_2O]^+$ (spectrum (b)) obtained from the irradiated estrone solution. The $[M_{ox}H-H_2O]^+$ ion (*m/z* 269) loses a water molecule leading to *m/z* 251, which leads to the formation of the ions at *m/z* 157 and 183 (Fig. 5(c)) also observed in the CID mass spectrum of $[\mathbf{1}H-H_2O]^+$. These ions are considered to be characteristic of ring A, and we concluded from the absence of any noticeable change in their *m/z* values that ring A of the steroid skeletal has not been modified. The formation of these ions has been explained in Scheme 2 and a proposed structure for the *m/z* 157 ion is given in Scheme 3. In both cases, the formation of these ions implies elimination of C_2H_4 involving the C6 and C7 carbon atoms. As none of these ions are shifted in their *m/z* values, we conclude that in the formation of these ions the part of the molecule that includes the modification has been expelled.

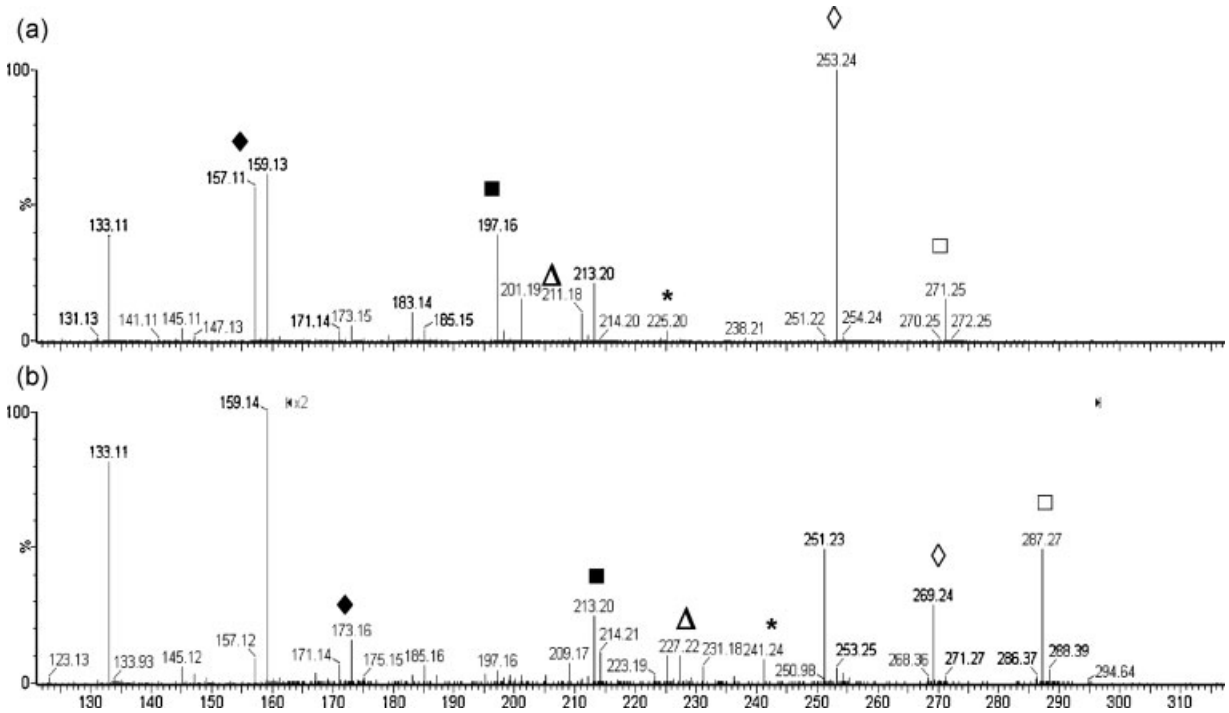

Figure 4. Comparison of the CID mass spectra of the *m/z* 271 ion (MH^+ of estrone at 6 min in the chromatogram (a) Fig. 3(a)) (a) and of the *m/z* 287 ion ($[M_{ox}]H^+$) at 2.48 min in the chromatogram (b) Fig. 3(b) for irradiated estrone. The various forms mark ions shifted by 16 *m/z* units from chromatogram (a) to (b).

DOI: 10.1002/rcm

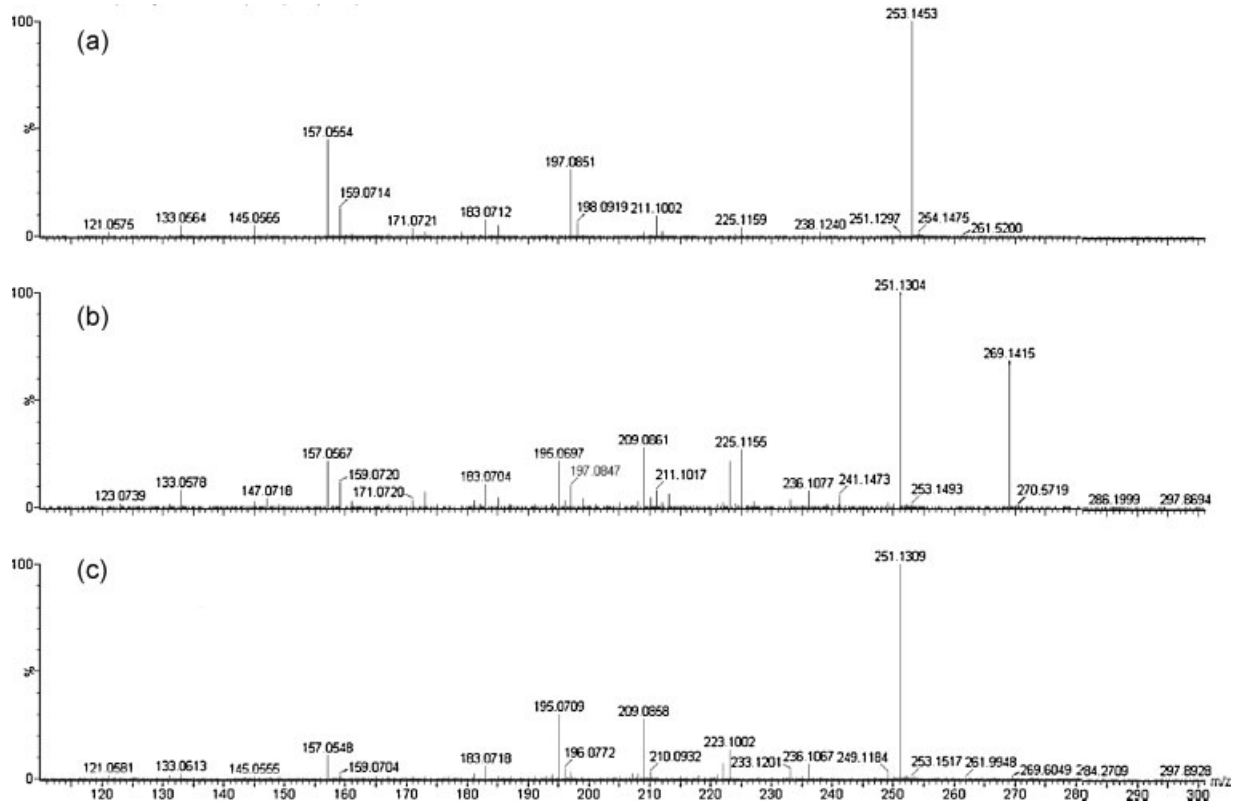

Figure 5. Comparison of the CID mass spectrum of $[MH^+-H_2O]$ of estrone at 6 min (a) and those of $[M_{ox}H^+-H_2O]$ (b) and $[M_{ox}H^+-2H_2O]$ (c) of the $M_{ox}H^+$ ion at *m/z* 287 obtained at 2.48 min for the irradiated estrone solution.

We thus suggest that the oxidation takes place at C6 or C7. Moreover, other ions in the spectrum are observed at *m/z* values shifted by –2 *m/z* units: *m/z* 195 (*m/z* 197 – 2); 209 (*m/z* 211 – 2); 223 (*m/z* 225 – 2); and -251 (*m/z* 253 – 2). This mass shift of 2 *m/z* units in the product ions could be attributed to the formation of an unsaturation through the first water elimination. This is consistent with the increase in DBE (double-bond equivalency, see Table 4). In particular, formation of a double bond could be rationalized by initial protonation of the $M_{ox}H^+$ photoproduct on a hydroxyl group present on the aromatic ring B (C6 or C7). The loss of water from this protonated species yields the *m/z* 269 product ion, which fragments similarly to *m/z* 271 (Scheme 2). This example allows us to propose two structures (see Fig. 6) for the oxidized compound obtained at a retention time of 2.48 min in the chromatogram of irradiated estrone.

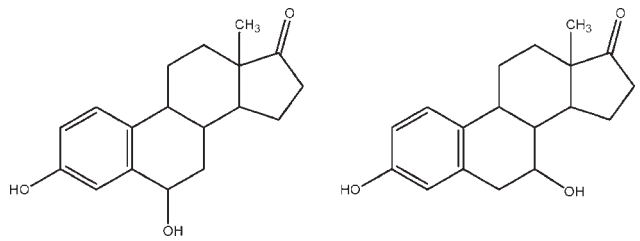

Figure 6. Structures of oxidized product of estrone obtained at 2.48 min.

Table 4. Accurate mass measurements of ions from the oxidized molecule detected at 2.48 min in the chromatogram of irradiated estrone solution, and present in Fig. 4(b)

Ions *m/z*	Elemental composition	Experimental mass (*m/z*)	Theorical mass (*m/z*)	Error mDa	Error (ppm)	DBE[a]
ESI-P						
287	$C_{18}H_{23}O_3$	287.1642	287.1647	−0.5	−1.7	7.5
269	$C_{18}H_{21}O_2$	269.1548	269.1542	0.6	2.2	8.5
251	$C_{18}H_{19}O$	251.1431	251.1436	−0.5	−2.0	9.5
241	$C_{16}H_{17}O_2$	241.1219	241.1229	−1	−4.1	8.5
227	$C_{15}H_{15}O_2$	227.1079	227.1072	0.7	3.1	8.5
223	$C_{16}H_{15}O$	223.1123	223.1123	0	0	9.5
213	$C_{14}H_{13}O_2$	213.0915	213.0916	−0.1	−0.5	8.5
209	$C_{15}H_{13}O$	209.0972	209.0966	0.6	2.9	9.5
195	$C_{14}H_{11}O$	195.0813	195.0810	0.3	1.5	9.5
173	$C_{11}H_9O_2$	173.0608	173.0603	0.5	2.9	7.5

[a] DBE: Double-bond equivalency.

CONCLUSIONS

The characterization of protonated and deprotonated estrone fragmentation pathways has been achieved using two standard molecules, estrone methyl ether (CH_3-E1) and deuterated estrone (E1-d_4). Two ESI-MS/MS acquisition modes have been compared for the analysis of these compounds. Positive ion and negative ion modes give information on both the protonated and deprotonated molecules and their product ions. In the negative ion mode, only one product ion was obtained, permitting us to

DOI: 10.1002/rcm

characterize the absence of modifications in rings A and B. On the other hand, the positive ion mode yielded more fragmentation and the resulting product ions were shown to be useful for characterizing structural modifications induced by photolysis on each ring of the estrone molecule. This mechanistic study has been successfully used for the identification of a photolysis compound, thus illustrating the benefit of mechanistic studies in identifying degradation products. These results are very promising for the determination of new metabolites in environmental matrices.

REFERENCES

1. Colborn T, Saal FSV, Soto AM. *Environ. Health Perspect.* 1993; **101**: 378.
2. Roda A, Mirasoli M, Michelini E, Magliulo M, Simoni P, Guardigli M, Curini R, Sergi M, Marino A. *Anal. Bioanal. Chem.* 2006; **385**: 742.
3. Richardson SD. *Anal. Chem.* 2008; **80**: 4373.
4. Lazarova V, Savoye P. *Water Sci. Technol.* 2004; **50**: 203.
5. Chen HC, Kuo HW, Ding WH. *Chemosphere* 2009; **74**: 508.
6. Albini A, Fasani E. In *Photochemistry and Photostability, Photochemistry of Drugs: An Overview and Practical Problems*. Royal Society of Chemistry: 1998.
7. Sun QF, Deng SB, Huang J, Shen G, Yu G. *Environ. Toxicol. Pharmacol.* 2008; **25**: 20.
8. Isobe T, Shiraishi H, Yasuda M, Shinoda A, Suzuki H, Morita M. *J. Chromatogr. A* 2003; **984**: 195.
9. Salvador A, Moretton C, Piram A, Faure R. *J. Chromatogr. A* 2007; **1145**: 102.
10. Zhang ZL, Hibberd A, Zhou JL. *Anal. Chim. Acta* 2006; **577**: 52.
11. Pedrouzo M, Borrull F, Marce RM, Pocurull E. *J. Chromatogr. A* 2009; **1216**: 6994.
12. Koha YKK, Chiu TY, Boobis A, Cartmell E, Lester JN, Scrimshaw MD. *J. Chromatogr. A* 2007; **1173**: 81.
13. Desbrow C, Routledge EJ, Brighty GC, Sumpter JP, Waldock M. *Environ. Sci. Technol.* 1998; **32**: 1549.
14. Kinani S, Bouchonnet S, Creusot N, Bourcier S, Balaguer P, Porcher J-M, Ait-Aissa S. *Environ. Pollut.* 2010; **158**: 74.
15. Pozo OJ, Van Eenoo P, Deventer K, Lootens L, Grimalt S, Sancho JV, Hernandez F, Meuleman P, Leroux-Roels G, Delbeke FT. *Steroids* 2009; **74**: 837.
16. Díaz M, Luiz M, Alegretti P, Furlong J, Amat-Guerri F, Massad W, Criado S, García NA. *J. Photochem. Photobiol. A* 2009; **202**: 221.
17. Zhao Y, Hu J, Jin W. *Environ. Sci. Technol.* 2008; **42**: 5277.
18. Irmak S, Erbatur O, Akgerman A. *J. Hazard. Mater.* 2005; **126**: 54.
19. Mazellier P, Meite L, De Laat J. *Chemosphere* 2008; **73**: 1216.
20. Hsu JF, Chang YC, Chen TH, Lin LC, Liao PC. *J. Chromatogr. B* 2007; **860**: 49.
21. Lagana A, Bacaloni A, Fago G, Marino A. *Rapid Commun. Mass Spectrom.* 2000; **14**: 401.
22. Quintanilla E, Davalos JZ, Abboud JLM, Alcami M, Cabildo MP, Claramunt RM, Elguero J, Mo O, Yanez M. *Chemistry - A European Journal* 2005; **11**: 1826.
23. Skotnicka-Pitak J, Garcia EM, Pitak M, Aga DS. *TrAC, Trends Anal. Chem.* 2008; **27**: 1036.

DOI: 10.1002/rcm

Human and Experimental Toxicology
1–12

DOI: 10.1177/0960327113493297
het.sagepub.com

Antioxidant status in rat kidneys after coexposure to uranium and gentamicin

C Poisson, C Rouas, L Manens, I Dublineau and Y Gueguen

Abstract

Uranium (U) accumulates and produces its toxic effects preferentially in the kidneys, especially in the proximal tubular structure. U disturbs the balance of pro-/antioxidants in the renal cortex after acute exposure. Other nephrotoxic agents, such as medications, also cause oxidative stress, but the effects of coexposure are not known. The aim of this study was to analyze the effect of chronic exposure to U and acute gentamicin treatment on the pro- and antioxidant status of the renal cortex of rats. Animals were chronically exposed (9 months) to a nonnephrotoxic level of U (40 mg/L) and then treated with daily injections of gentamicin at a range of doses (0, 5, 25, 100, and 150 mg/kg) during the last week of contamination. We studied changes in the gene expression, protein expression, and enzyme activity of key factors involved in the pro-/antioxidant balance in the renal cortex. At and above a dose of 100 mg/kg, gentamicin decreased the messenger RNA (mRNA) levels of catalase (*CAT*), copper/zinc superoxide dismutase (*SOD*) and increased the mRNA levels of *heme oxygenase-1* in contaminated rats. This treatment decreased CAT activity, but did not significantly change the SOD protein level. Chronic exposure to U did not worsen these effects in our experimental conditions. In conclusion, gentamicin treatment disturbed the oxidative balance in our model's renal cortex, but the chronic exposure to U at this nonnephrotoxic level did not appear to reinforce these effects.

Keywords

Depleted uranium, gentamicin, oxidative stress, chronic exposure, kidney

Introduction

Uranium (U), because it is both naturally present in the earth's crust and used by humans for various purposes, is found in the environment, where exposure to it presents risks to local populations. Because of their properties as heavy metals, both natural and depleted U (DU), a by-product of enriched U, are toxic chemicals. In view of its low specific radioactivity, this toxicity dominates its adverse effects on humans. The kidneys are the major target of acute U toxicity.[1] Chronic exposure produces functional kidney changes in humans,[2] and morphological and functional modifications of the proximal tubular cells of rats.[3,4]

Induced oxidative stress is one of the principal explanations for these disturbances. It is a common cause of kidney failure induced by numerous metals, including mercury, chromium, cadmium (Cd), and iron[5] as well as U.[6] Oxidative stress is caused by an imbalance between the production of reactive oxygen species (ROS) and a biological system's ability to detoxify the reactive intermediates or repair the resulting damage easily. Under stress or toxic conditions, ROS product ions can lead to lipid peroxidation, DNA alteration, or sugar oxidation. Cell and tissue functions can be impaired, resulting in various chronic diseases such as kidney failure, diabetes, atherosclerosis, and Alzheimer's disease.

The body's antioxidant defense system includes various actors, including enzymes (both catalase (CAT)

Institut de Radioprotection et de Sureté Nucléaire (IRSN), PRP-HOM, SRBE, LRTOX, Fontenay-aux-Roses, France

Corresponding author:
Yann Gueguen, Institut de Radioprotection et de Sûreté Nucléaire (IRSN), PRP-Hom, SRBE, Laboratoire de RadioToxicologie Expérimentale. B.P. n°17, Fontenay-aux-Roses Cedex 92262, France.
Email: yann.gueguen@irsn.fr

and superoxide dismutase (SOD)), glutathione (GSH),[7] and transcription factors such as NF-E2-related factor (Nrf2).[8] Lestaevel et al. studied the antioxidant system involved in the brain effects of chronic exposure to U and showed that it induced gene expression of the principal antioxidant enzymes, such as CAT or SOD.[9] However, the effects of chronic exposure on the kidneys have not yet been shown.

Indeed, few published studies have described the in vivo oxidative stress status of the kidneys after chronic exposure to U.[10] No study has examined the effects on oxidative stress of U exposure combined with other nephrotoxic xenobiotics such as gentamicin. In a previous study, we have shown that those renal tubular necrosis were aggravated in DU-exposed rats treated with the highest gentamicin concentration.[11] These alterations were not confirmed by specific nephrotoxic biomarkers analysis (such as kallikrein or Kidney Injury Molecular 1(KIM-1)). But, oxidative stress being a common marker of exposure to DU and gentamicin, it is important to pursue this work by studying the effects of DU and gentamicin coexposure on the pro-/antioxidative system in the renal cortex. Indeed, different mechanisms are known to cause gentamicin nephrotoxicity, but the induction of oxidative stress has been studied in most detail. Gentamicin is an aminoglycoside antibiotic commonly prescribed to treat gram-negative infections, and its nephrotoxicity is well established.[12,13] In the nephron, its target is the proximal tubular cells.[14] Cuzzocrea et al. reports that SOD, an antioxidant enzyme, plays a key role in gentamicin-mediated nephropathy.[15] Similarly, Silan et al. showed that ROS also has a role in gentamicin-induced kidney injury.[12]

The objective of this study was to determine whether rats coexposed to DU and gentamicin developed signs of oxidative stress in the kidneys. Adult male rats were exposed for 9 months to a nonnephrotoxic dose (40 mg/L) of DU and were then treated with increasing doses of gentamicin (0, 5, 25, 100, and 150 mg/kg) during the last week of DU exposure.

To assess nephrotoxicity and oxidative status, we studied the following variables in the renal cortex of rats: standard indicators of kidney dysfunction (urea, creatinine, and creatinine clearance) and lipid peroxidation (by measuring thiobarbituric acid reactive substances (TBARS)), as well as the gene, protein, and activity levels of various antioxidant enzymes (CAT, copper-/zinc-SOD (Cu/Zn-SOD) and manganese SOD (Mn-SOD), glutathione peroxidase (GPx), glutathione reductase (GR), and heme oxygenase-1(HO-1)).

Materials and methods

Animals

The study was performed on Sprague Dawley rats provided by Charles River (L'Arbresle, France). Animals were housed in pairs with a 12-h light/12-h dark cycle and under constant room temperature condition ($21 \pm 1°C$). The study was approved by the IRSN Animal Care Committee and conducted in accordance with French regulations for animal experimentation (Ministry of Agriculture Act No. 2011-110, June 2011).

Experimental design

Animal DU exposure. The rats in the contaminated group were exposed via their drinking water to depleted uranyl nitrate (^{238}U: 99.74%, ^{235}U: 0.26%, and ^{234}U: 0. 001%; AREVA-NC Pierrelatte, France) for 9 months at a dose of 40 mg/L (about 1 mg/kg/day). This dose is equivalent to twice the highest concentration found naturally in well water in Finland.[16] Control animals drank no contaminated water. Each group contained 40 animals (Figure 1).

Animal gentamicin treatment. During the last week of U exposure, all the rats in both groups (DU-exposed or not exposed (NE)) received gentamicin or vehicle (sodium chloride (NaCl) 0.9%) treatment (Figure 1). The gentamicin sulfate (Sigma Aldrich, Lyon, France) was administered by subcutaneous injection for four consecutive days (either 0, 5, 25, 100, or 150 mg gentamicin per kilogram of body weight) in 0.9% NaCl, injected at a volume of 1 mL/kg ($n = 8$ for each condition). The rats were weighed daily during the week of gentamicin treatment.

Kidney collection, preparation, and conservation. Animals were anesthetized by inhalation of isoflurane and then euthanized by intracardiac puncture. Both kidneys were collected and weighed for each rat. The cortex and the medulla were meticulously separated, flash frozen in liquid nitrogen, and stored at $-80°C$. All substances were measured in the renal cortex, which is the principal kidney site for the accumulation of both U[17] and gentamicin.[15]

Plasma and urine analysis. Blood was centrifuged at 4000*g* for 10 min (4°C) to obtain plasma in heparin tube and serum that were stored at $-80°C$. Urine was collected for 24 h after the last gentamicin injection

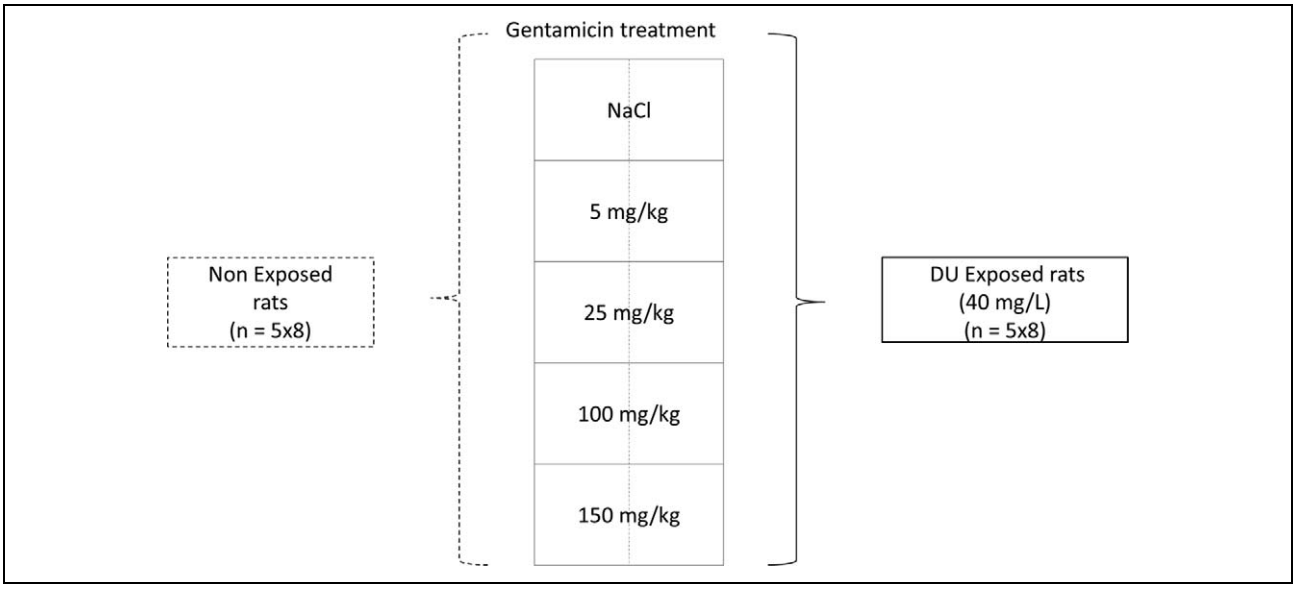

Figure 1. Groups of rats exposed (DU) or not (NE) to uranium and treated by increasing concentration of gentamicin (5–150 mg/kg) or 0.9% NaCl. DU: depleted uranium; NE: not exposed; NaCl: sodium chloride.

Table 1. Primer sequences for gene encoding antioxidatives enzymes.

Gene	Forward	Reverse	Reference
HPRT	5′-GCT CGA GAT GTC ATG AAG GAG A-3′	5′-TCA GCG CTT TAA TGT AAT CCA GC-3′	18
Cu/Zn SOD	5′-GAT TAA CTG AAG GCG AGC AT-3′	5′-CCG CCA TGT TTC TTA GAG T-3′	19
Mn-SOD	5′-ACG CGA CCT ACG TGA ACA ATCT-3′	5′-CAG TGC AGG CTG AAG AGC AA-3′	20
GPx	5′-TGC AAT CAG TTC GGA CAT CA-3′	5′-ACC ATT CAC CTC GCA CTT C-3′	19
CAT	5′-GAG AGG AAA CGC CTG TGT GAG-3′	5′-AAG AGC CTG GAC TCG GGC CC-3′	21
GR	5′-TTG CTG GCC TCT ATT CAC TGG A-3′	5′-ATT ACC TCC GCC CTC TCT TTG-3′	This study
HO-1	5′-ATG CCC CAC TCT ACT TCC CTG A-3′	5′-TGC TGT GTG GCT GGT GTG TAA G-3′	This study

HPRT: hypoxanthine–guanine phosphoribosyltransferase; HO-1: heme oxygenase-1; Cu-/Zn-SOD: copper/zinc sodium dismutase; Mn-SOD: manganese sodium dismutase; GPx: glutathione peroxidase; CAT: catalase.

and then centrifuged at 3000*g* for 10 min (4°C). The supernatants were collected and stored at −80°C.

The levels of gentamicin, creatinine, and urea in plasma and of gentamicin and creatinine in urine were measured with an automated Konelab 20 analyzer (Thermo Scientific, Cergy-Pontoise, France) (all biological chemistry reagents were obtained from ThermoElectron (Thermo Fischer Scientific, Illkirch, France)). Creatinine clearance was calculated according to this equation

$$\begin{aligned}&\text{Creatinine clearance } (\mu\text{mol/L/kg})\\&\quad = [(\text{urinary creatinine } (\mu\text{M})/\text{diuresis } (\text{mL/min}))\\&\qquad \times \text{plasmacreatinine}(\mu\text{M}]/\text{weight}(\text{kg})\end{aligned}$$

Gene expression analysis. Total RNA from the cortex renal was prepared with the RNeasy Total RNA isolation kit (Qiagen, Courtaboeuf, France), according to the manufacturer's instructions. High-capacity complementary DNA (cDNA) reverse transcription kits (Life Technologies, Villebon-sur-Yvette, France) were used for the reverse transcription.

Real-time polymerase chain reactions (PCRs) were used to analyze the messenger RNA (mRNA) levels of enzymes involved in the oxidative balance: CAT, GPx, GR, HO-1, Mn-SOD, and Cu-/Zn-SOD. Table 1 reports the sequences for the forward and reverse primers used in this study. In each well, the total volume (10 µL) was adjusted to reach a final concentration of

1 ng/μL of cDNA, with 83% v/v SYBR (Life Technologies), 14.5% v/v sterile water, and 2.5% v/v primers (Life Technologies). Optimized PCR used the AbiPrism 7900 Sequence Detection System (Life Technologies). Samples were normalized to the housekeeping gene, hypoxanthine–guanine phosphoribosyltransferase (HPRT).

Western blot. Mn-SOD, Cu/Zn-SOD, and HO-1 were semiquantified by Western blotting. Proteins from renal cortex homogenate underwent 10% sodium dodecyl sulfate polyacrylamide gel (SDS-PAGE) electrophoresis and were blotted onto a nitrocellulose membrane. After blocking with 5% nonfat dry milk in Tris Buffered Saline (TBS) for 1 h, the blots were incubated overnight with a primary antibody diluted in 2% nonfat dry milk in TBS at 4°C. Anti-Cu-/Zn-SOD and anti-Mn-SOD polyclonal rabbit antibodies (Merck Millipore, Molsheim, France) and anti-HO-1 polyclonal goat antibody (Santa Cruz Biotechnology, Heidelberg, Germany) were diluted at 1:500, 1:2000, and 1:200, respectively. Immune complexes were revealed by goat anti-rabbit or rabbit anti-goat immunoglobulin G (Santa Cruz Biotechnology) coupled to horseradish peroxidase and luminol-based derivative of Immobilon Western (Merck Millipore). Band densities were quantified with a camera and computer-assisted densitometry (Fuji Las3000, Raytest, Paris, France) and normalized to glyceraldehyde-3-phosphate dehydrogenase or beta-actin (β-actin) detected, respectively, with rabbit anti-goat or goat anti-mouse antibody (Santa Cruz Biotechnology).

Analysis of enzymatic activities. For each assay, 25 mg of renal cortex was homogenized in 10 volumes of appropriate buffer (for CAT and GPx, sample buffer was provided by the manufacturer and for GR, the buffer used was composed of 50 mM potassium phosphate, pH 6–7, and ethylenediaminetetraacetic acid, 1 mM). Tissue samples were then centrifuged at 12,000*g* for 10 min at 4°C, and the supernatants collected for analyses. Protein concentrations were determined by the Bradford method with serum albumin as the standard.

CAT, GPx, and GR activities were determined with commercial kits supplied by Cayman Chemical (Bertin Pharma, Montigny-le-Bretonneux, France). CAT activity, expressed in nanomoles per minute per milligram of proteins, was assessed via its peroxidatic function, with formaldehyde formation measured spectrophotometrically with a chromogen. GPx activity was assessed indirectly by coupled reaction with GR; the oxidized GSH was recycled to its reduced state by GR and NADPH. NADPH oxidation is accompanied by decreased absorbance at 340 nm directly proportional to GPx activity in the sample. The activity was expressed in nanomoles per minute per microgram of proteins. GR was measured by the NADPH oxidation rate. Its oxidation is also accompanied by decreased absorbance at 340 nm, directly proportional to GR activity in the sample. Results were expressed in nanomoles per minute per microgram of proteins.

Lipid peroxidation. Lipid peroxidation was evaluated by measuring TBARS with a commercial kit supplied by Cayman Chemical (Bertin Pharma). This kit used the reaction between malondialdehyde (MDA) and thiobarbituric acid (TBA) at high temperatures (90–100°C) and acidic conditions to form MDA-TBA and water, measured spectrophotometrically at 530–540 nm.

Statistical analysis

A two-way analysis of variance test was used. The two groups differed according to their exposure to DU (DU and NE). Half the rats in each of these groups were exposed to gentamicin. All results were expressed as mean ± SEM. Statistical software Sigma Plot 11.0 (SPSS, France) was used for all statistical analysis. The level of significance was set at $p < 0.05$.

Results

Kidney biochemical parameters

Kidney function for all animals was evaluated by standard markers: plasma creatinine and urea and creatinine clearance. No significant effect was observed at doses below 100 mg/kg of gentamicin for DU and NE groups. Plasma urea and creatinine levels increased, as evidenced by the nephrotoxicity ($p < 0.001$), at doses higher than 100 mg/kg of gentamicin. This increase began at that level in both the DU and NE groups. In NE rats, the increase was significant for both urea and creatinine (by factors of 1.8 and 1.5, respectively, $p < 0.01$ for both; Figure 2). In DU rats, on the other hand, at the highest dose of gentamicin, only plasma creatinine increased, to a level 1.5 times higher than in the control group (DU without gentamicin).

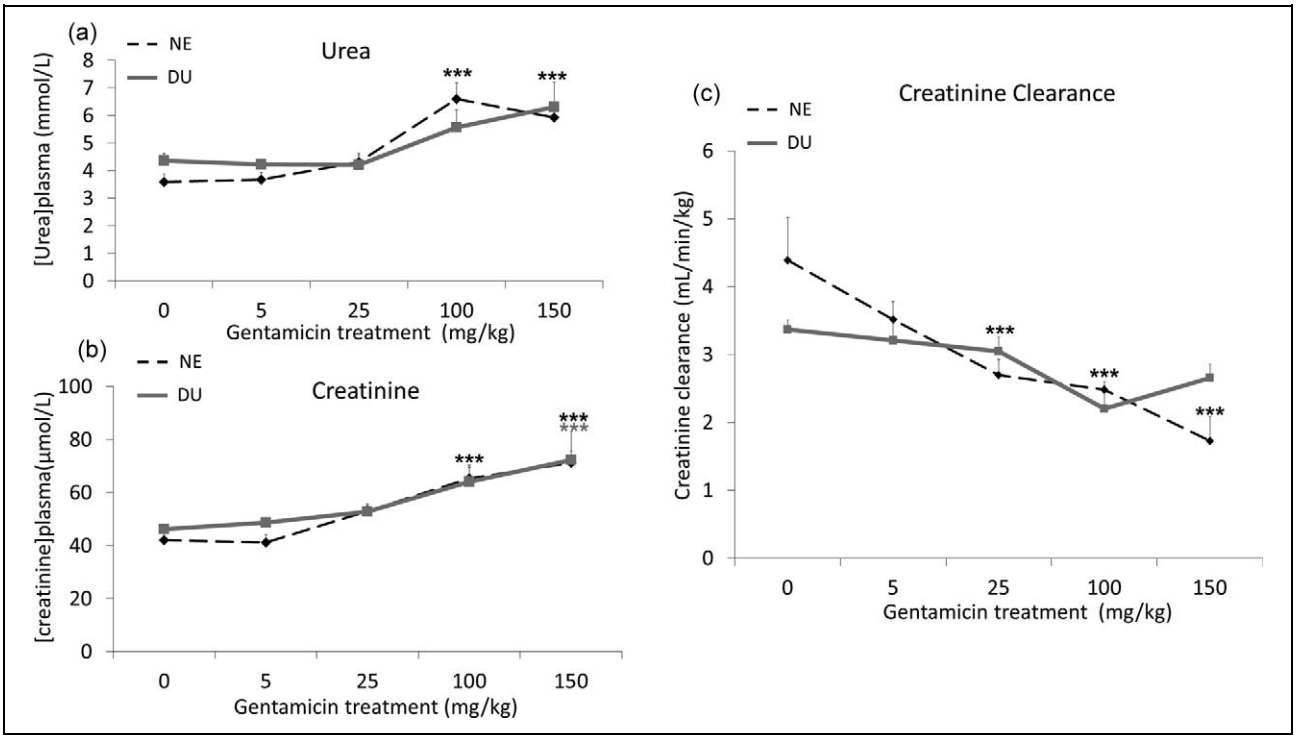

Figure 2. Kidney physiological and plasmatic parameters in nonexposed (NE) and in DU-exposed (DU) rats treated or not by gentamicin (5–150 mg/kg) for 4 days. Asterisk represents a significant difference between gentamicin treated and untreated (0) rats ($n = 8$ for each group; two-way analysis of variance, ***$p < 0.001$). DU: depleted uranium; NE: not exposed.

Accordingly, exposure to U had no effect on plasma urea or creatinine.

A dose-dependent reduction in creatinine clearance was observed for NE rats exposed to gentamicin from 25 mg/kg. Creatinine clearance also decreased in DU rats, and gentamicin treatment had no significant effect on this parameter for DU rats. These kidney changes showed that gentamicin treatment disrupted kidney integrity.

Antioxidant enzymes

Gene expression and enzymatic activity were studied for the major enzymes involved in the pro-/antioxidant balance in the renal cortex. In normal conditions, antioxidant enzymes are mainly found in this part of the nephron.[15]

The figures present mRNA quantity (in arbitrary units), activity (nanomoles per minute per milligram or nanomoles per minute per microgram), and protein levels (arbitrary units), according to gentamicin treatment (in milligrams per kilogram). The dotted black line represents the NE group and the continuous gray line the DU group.

Catalase. Figure 3(a) shows a significant decrease in CAT gene expression, at a dose of 100 mg/kg gentamicin in both NE and DU-exposed rats (64%, $p < 0.01$). CAT enzymatic activity (Figure 3(b)) decreased significantly from 5 mg/kg gentamicin for the NE rats (by a factor of 1.8, $p < 0.001$) and from 100 mg/kg gentamicin for the DU rats (again, by a factor 1.8, $p < 0.01$). Gentamicin treatment induced a dose-dependent decrease in CAT activity, while the effect of DU exposure was not cumulative with that of gentamicin.

Glutathione peroxidase. As shown in Figure 4(a), gene expression of *GPx* did not change until the gentamicin dose reached 100 mg/kg in NE rats (i.e. at 100 mg/kg of gentamicin for NE rats (−57%, $p < 0.01$)). Regardless of the gentamicin dose, the *GPx* level did not differ between DU-exposed and NE rats. Nor did GPx activity (Figure 4(b)) differ with gentamicin treatment or U exposure.

Glutathione reductase. GR gene expression did not differ significantly after either gentamicin treatment or

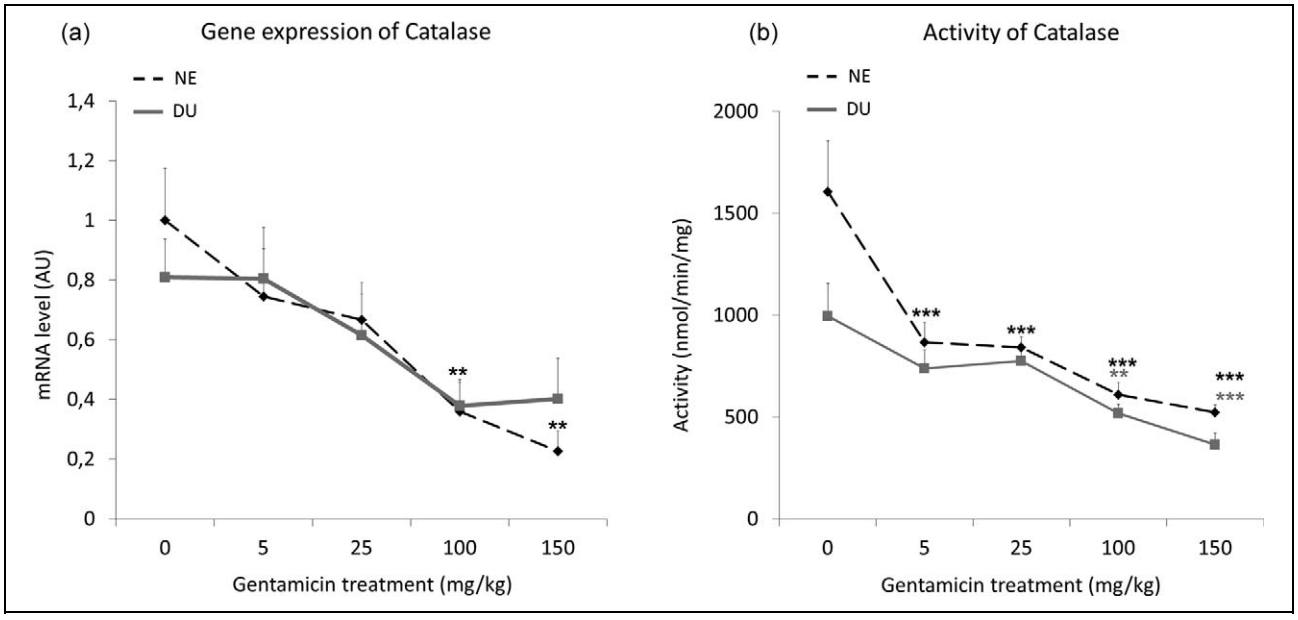

Figure 3. Catalase gene expression (a) and activity (b) in renal cortex of kidney in nonexposed (NE) and in DU-exposed (DU) rats treated or not by gentamicin (5–150 mg/kg) for 4 days ($n = 8$ for each group). The ratio is expressed as a ratio of the mRNA levels of housekeeping gene hypoxanthine–guanine phosphoribosyl transferase, in AU. The activity is expressed in nanomoles per minute per milligram of proteins. Asterisk represents a significant difference between gentamicin treated and untreated (0) rats (two-way analysis of variance, $^{**}p < 0.01$, $^{***}p < 0.001$). DU: depleted uranium; NE: not exposed; AU: arbitrary units; mRNA: messenger RNA.

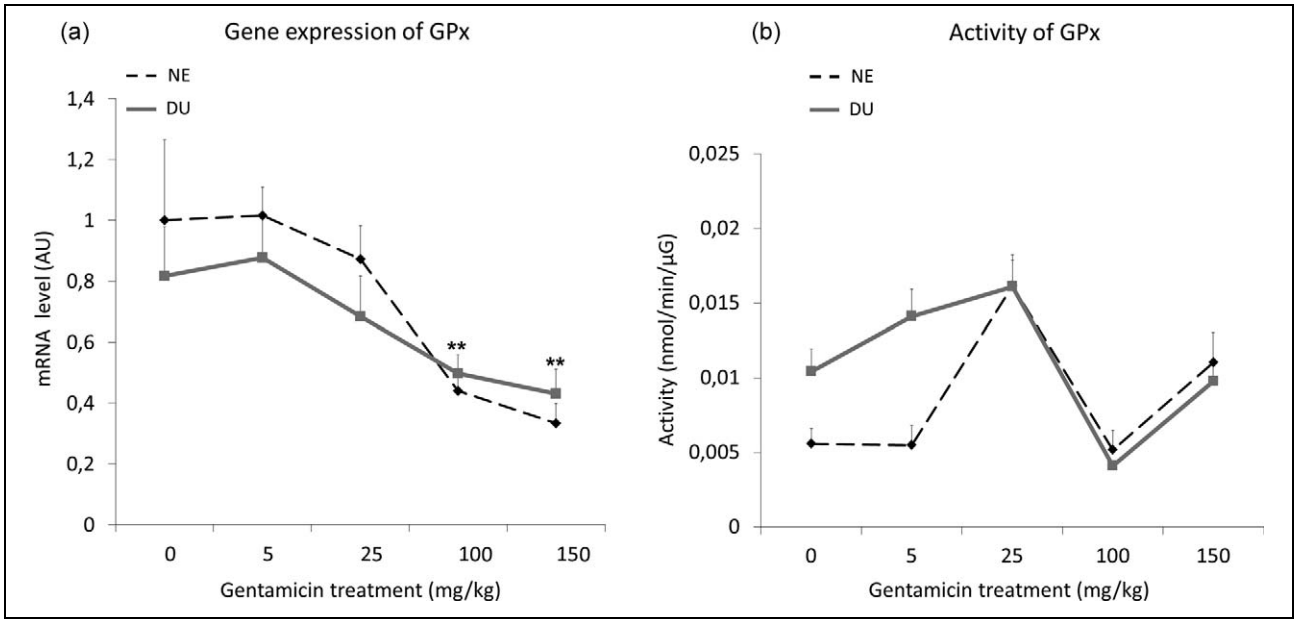

Figure 4. Glutathione peroxidase gene expression (a) and activity (b) in renal cortex of kidney in nonexposed (NE) and in DU-exposed (DU) rats treated or not by gentamicin (5–150 mg/kg) for 4 days ($n = 8$ for each group). The ratio is expressed as a ratio of the mRNA levels of housekeeping gene hypoxanthine–guanine phosphoribosyl transferase, in AU. The activity is expressed in nanomoles per minute per microgram of proteins. Asterisk represents a significant difference between gentamicin treated and untreated (0) rats (two-way analysis of variance, $^{**}p < 0.01$). DU: depleted uranium; NE: not exposed; AU: arbitrary units; mRNA: messenger RNA.

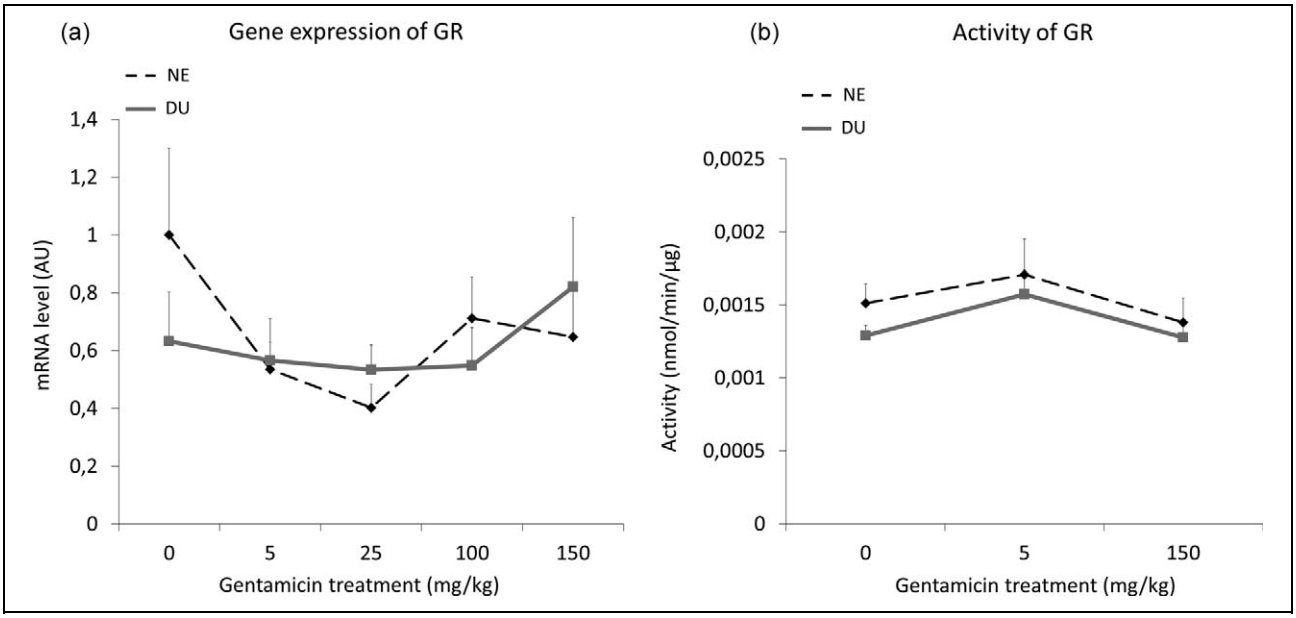

Figure 5. Glutathione reductase gene expression (a) and activity (b) in renal cortex of kidney in nonexposed (NE) and in DU-exposed (DU) rats treated or not by gentamicin (5–150 mg/kg) for 4 days ($n = 8$ for each group). The ratio is expressed as a ratio of the mRNA levels of housekeeping gene hypoxanthine–guanine phosphoribosyl transferase, in AU. The activity is expressed in nanomoles per minute per microgram of proteins. DU: depleted uranium; NE: not exposed; AU: arbitrary units; mRNA: messenger RNA.

DU exposure, as shown in Figure 5. Similarly, neither exposure affected GR enzymatic activity.

Superoxide dismutases. These metalloenzymes catalyze the dismutation of superoxide anion into hydrogen peroxide and molecular oxygen. There are two principal types of SOD: Cu/Zn-SOD is found in the cytosol and Mn-SOD mainly in the mitochondria.

Mn-SOD. Neither gentamicin treatment nor exposure to U appeared to have any significant effect on either the gene expression or protein levels of Mn-SOD (Figure 6).

Cu/Zn-SOD. Gene expression of *Cu/Zn-SOD* (Figure 7) decreased significantly NE animals at the highest gentamicin dose (by factors of 2.7, $p < 0.001$). On the other hand, a significant effect was observed from U exposure in rats treated with 100 mg/kg gentamicin ($p < 0.05$). Nevertheless, neither gentamicin treatment nor exposure to DU significantly modified protein levels of this enzyme.

Heme oxygenase-1. As shown in Figure 8(a), *HO-1* gene expression increased significantly in rats treated with 100 mg/kg of gentamicin in both the DU and NE groups. The protein level did not differ in any of the experimental groups (Figure 8(b)).

Lipid peroxidation

We measured TBARS to assess lipid peroxidation. They did not vary significantly in any of the groups considered: DU versus NE rats or gentamicin versus NaCl treatment (Figure 9).

Discussion

It has been clearly established that U is a nephrotoxic agent[1,22] and that the first symptom of this toxicity is tubular nephritis.[1,23,24] The physiological mechanism underlying this renal damage has nonetheless not been completely elucidated. One of the mechanisms for this nephrotoxic action of U mentioned most often is an imbalance in the oxidative status of the kidneys,[6] more precisely in the renal cortex of the nephron, and specifically in the renal proximal tubular cell.[24,25] Increased lipid peroxidation in the renal cortex was observed in rats after intraperitoneal (i.p.) injection of 0.5 mg/kg uranyl nitrate for 5 days.[24] After contamination of mice by i.p. injection (0.5 mg/kg) of uranyl nitrate for 2 days, Taulan et al. reported some changes in the levels of the antioxidant enzymes SOD and GPx, which are involved in oxidative equilibrium.[26]

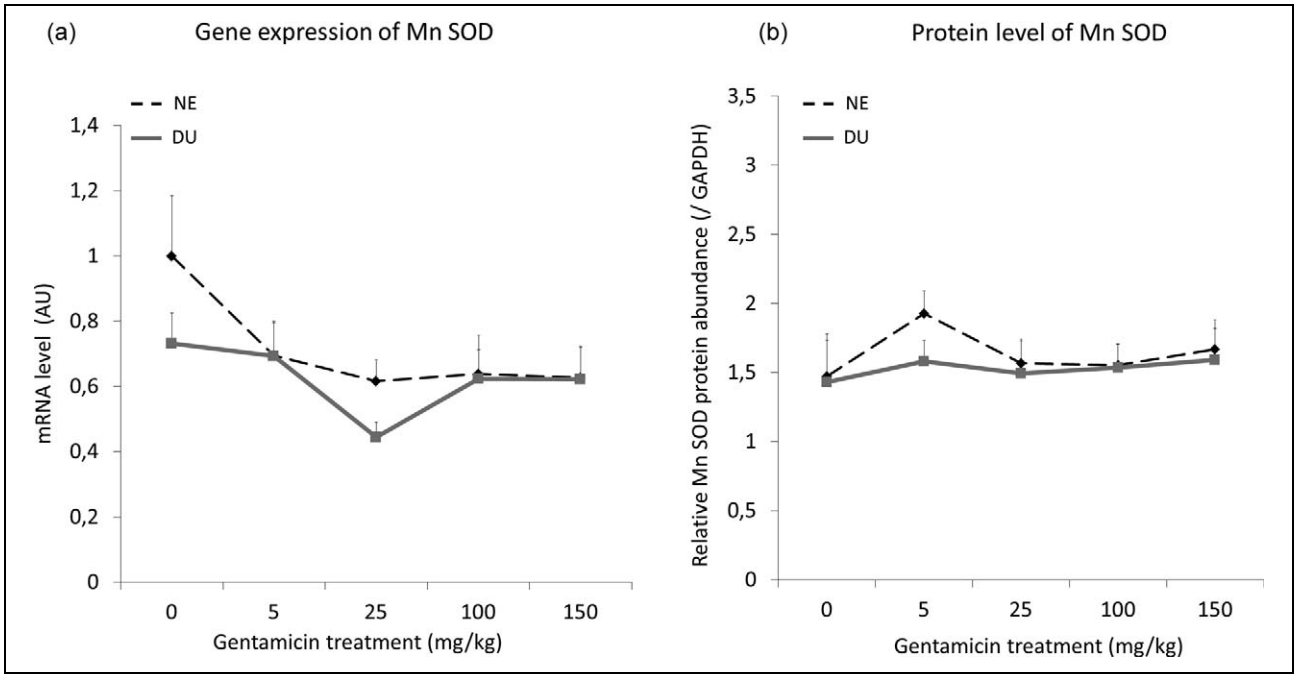

Figure 6. Mn-SOD gene expression (a) and protein levels (b) in renal cortex of nonexposed and in DU-exposed rats treated or not by gentamicin (5–150 mg/kg) for 4 days ($n = 8$ for each group). In (a), the ratio is expressed as a ratio of the mRNA levels of housekeeping gene hypoxanthine–guanine phosphoribosyl transferase, in AU. For Western blot (b), GAPDH was used as a loading control. Data are expressed as mean $\pm$ SEM of the target protein band intensity as compared to GAPDH band intensity. DU: depleted uranium; NE: not exposed; AU: arbitrary units; Mn-SOD: manganese sodium dismutase; GAPDH: glyceraldehyde-3-phosphate dehydrogenase; mRNA: messenger RNA.

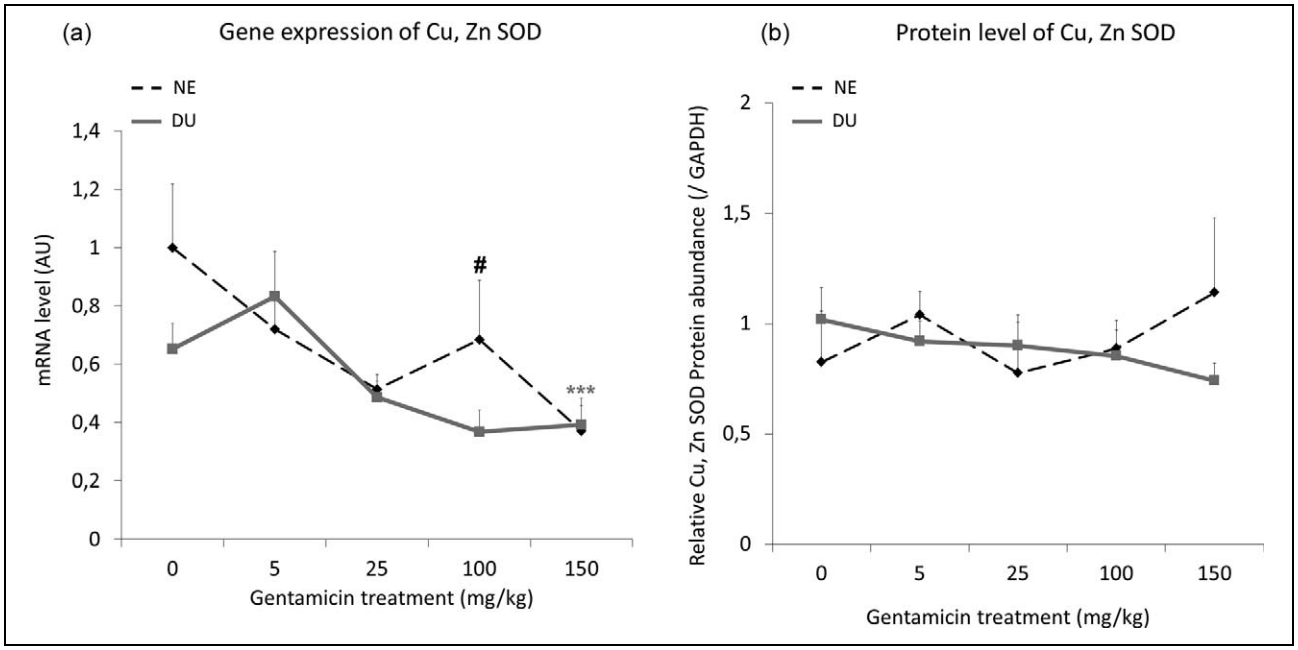

Figure 7. Cu-/Zn-SOD gene expression (a) and protein levels (b) in renal cortex of nonexposed and in DU-exposed rats treated or not by gentamicin (5–150 mg/kg) for 4 days. In (a), the ratio is expressed as a ratio of the mRNA levels of housekeeping gene hypoxanthine–guanine phosphoribosyl transferase, in AU. For Western blot (b), GAPDH was used as a loading control. Data are expressed as mean $\pm$ SEM of the target protein band intensity as compared to GAPDH band intensity, $n = 8$ for each group. Asterisk represents a significant difference between gentamicin treated and untreated (0) rats (two-way ANOVA, ***$p < 0.001$). Sharp sign represents a significant difference between DU exposed (DU) and nonexposed (NE) rats ($n = 8$ for each group; two-way ANOVA, #$p < 0.05$). DU: depleted uranium; NE: not exposed; AU: arbitrary units; Cu/Zn-SOD: copper/zinc sodium dismutase; GAPDH: glyceraldehyde-3-phosphate dehydrogenase; ANOVA: analysis of variance.

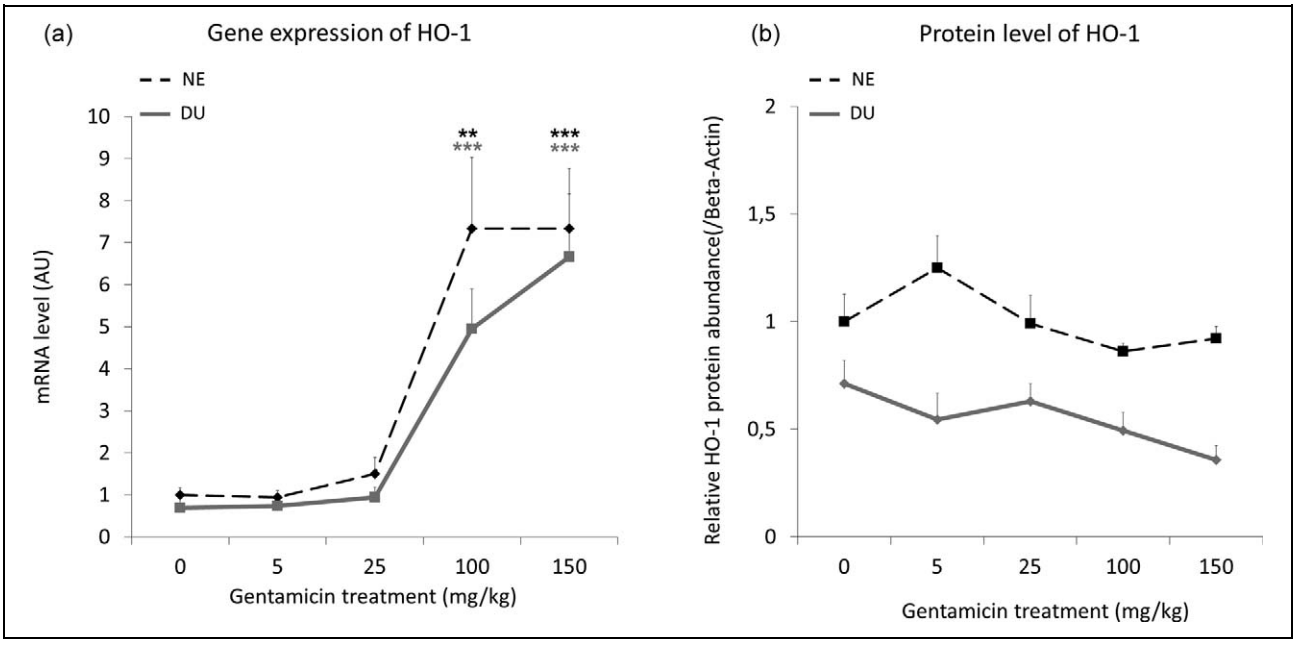

Figure 8. HO-1 gene expression in renal cortex of nonexposed and in DU-exposed rats treated or not by gentamicin (5–150 mg/kg) for 4 days ($n = 8$ for each group). In (a), the ratio is expressed as a ratio of the mRNA levels of housekeeping gene hypoxanthine–guanine phosphoribosyl transferase, in AU. For Western blot (b), beta-actin was used as a loading control. Data are expressed as mean $\pm$ SEM of the target protein band intensity as compared to beta-actin band intensity. Asterisk represents a significant difference between gentamicin treated and untreated (0) rats (two-way analysis of variance, $^{**}p < 0.01$, $^{***}p < 0.001$). DU: depleted uranium; NE: not exposed; AU: arbitrary units; HO-1: heme oxygenase-1; mRNA: messenger RNA.

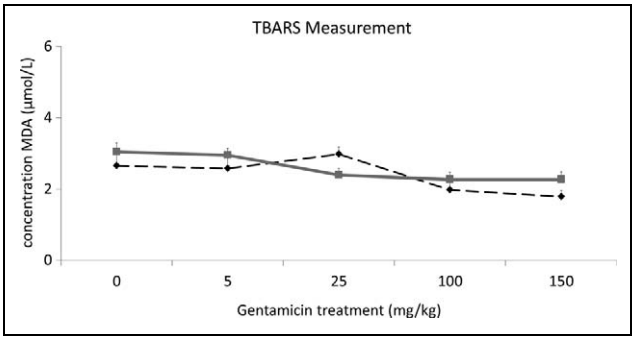

Figure 9. Evaluation of lipid peroxidation by TBARS measurement in renal cortex of nonexposed (NE) and in DU-exposed (DU) rats treated or not (0) by gentamicin (5–150 mg/kg) for 4 days ($n = 8$ for each group). Concentration of MDA is in micromoles per liter. DU: depleted uranium; NE: not exposed; TBARS: thiobarbituric acid reactive substances; MDA: malondialdehyde.

Increased oxidative stress has also been observed in other organs after acute exposure to uranyl nitrate, including the central nervous system (CNS), bones, and lungs.[27–29] Similar results are reported in other species: uranyl nitrate induces oxidative stress in the proximal tubular cells of rabbit kidneys[30] but also in the liver of Danio Rerio fish.[31] Such stress, however, has not been studied previously in the kidney of rodent after chronic exposure to a nonnephrotoxic U dose. In our work, U concentration in the kidneys was less than 0.15 µg/g of kidney, a nonnephrotoxic concentration.

Here, we used a rat model of chronic exposure developed in the laboratory[11] that enabled us to study simultaneously the effects of chronic exposure to U, acute gentamicin treatment and coexposure to these two potentially prooxidant agents. It is important to note that DU exposure induces any significant modification in the renal plasma biochemical parameters. These results are in line with previous studies conducted on rats exposed to 40 mg/L of DU during 9 months.[32,33]

To study if antioxidant status could be modified, we first analyzed lipid peroxidation (measured by the quantity of TBARS formed) in this model and found no significant change after chronic exposure. In comparison, after 3 months of contamination by increasing U concentrations (10–40 mg/kg),[10] no increase in TBARS activity was observed at the lowest dose, which was also the dose closest to that used in this study. But there was a significant increase at the highest concentration, almost 20 times higher than in our

study. This increase was correlated with the U concentration in the kidneys. The discrepancy between these studies can be explained by the U dose. Nonetheless, in the study by Linares et al., the renal activity of the antioxidant enzymes evaluated (GPx and GR) did not change as it did in this study.

The effect of chronic exposure to U on pro-/antioxidant status has been studied in other tissues, including the testes and the CNS. Linares et al.[10] found in another study that GR activity and GSH level decreased in the testis, while Lestaevel et al. showed increased activity of some antioxidant enzymes in the CNS.[9]

These enzymes are not altered by chronic exposure to U in the kidney at this dose, as mentioned previously in this text. So, adaptation mechanisms could occur beforehand.

These adaptation mechanisms have been reported in a review for various toxic substances.[34] Cd is another toxic heavy metal, which is also a nephrotoxic agent.[35] It can induce oxidative stress.[36–38] Both increased[36] and decreased lipid peroxidation[39] have been described after chronic Cd exposure. Other authors have shown a biphasic defense to low Cd concentrations, by activation of antioxidant enzymes in the kidneys of chronically exposed mice.[40] Liu et al. reviewed many studies of chronic Cd exposure and hypothesized that compensatory mechanism following the oxidative stress could be developed by the organism in response to Cd chronic exposure.[41] The similarities between Cd and U are that both are heavy metals, nephrotoxic agents, and inducers of oxidative stress; mechanisms of adaptation could appear after chronic exposure to U.

Like heavy metals, some drugs also induce oxidative stress. Gentamicin is a well-known nephrotoxic antibiotic[42] and one of the predominant mechanisms of this nephrotoxicity includes the induction of oxidative stress.[43] In our study, the use of increasing concentrations of gentamicin led to a dose-dependent pro-/antioxidant imbalance, demonstrated by decreased CAT activity and gene expression of *CAT* and *Cu/Zn-SOD.* In similar experimental conditions, decreased activities of the antioxidant enzymes CAT, SOD, and GPx were described.[44]

The two main isoforms of SOD were studied: Mn and Cu/Zn. Gene expression of *Cu/Zn-SOD* was altered by gentamicin treatment. These variations were not observed at the protein level. It suggested that the transcription of this gene encoding for these enzymes was disturbed by gentamicin treatment, whereas it had no effect on the protein translation.

Gene expression of *Cu/Zn-SOD* is significantly different between NE and DU groups only at a dose of 100 mg/kg of gentamicin, which is described as nephrotoxic.

In this work, it can be supposed that the difference in gene expression between both SOD isoforms is probably due to their cellular localization and the effect of gentamicin and U in the different cellular compartments. Indeed, Mn-SOD is mainly localized in the mitochondria, whereas Cu/Zn-SOD is found in the cytosol. Recently, we have shown in an in vitro study that the U distribution is heterogeneous between the nuclear and the cytoplasm,[45] but the U and gentamicin localization in different organelles is not yet known. Nevertheless, this result leads to suggest that U localization being heterogeneous, U effects on organelles are heterogeneous too, that could explain the different effects between Cu/Zn- and Mn-SOD.

As reported above, lipid peroxidation in our model did not vary with gentamicin treatment or exposure to U or both together. Other studies report that gentamicin induces TBARS production during longer treatment,[46] but coexposure to another xenobiotic was not studied. *HO-1,* which is another important antioxidant enzyme, was significantly induced starting at a dose of 100 mg/kg gentamicin in our model, as reported previously.[47] However, chronic exposure to U at a dose of 40 mg/L produced no synergistic effects.

Overall, according to our model, no potentiations of gentamicin's prooxidant effect were observed. Only some sporadic changes in the levels of antioxidant enzymes were observed due to U exposure, consistent with what has been reported previously about nephrotoxicity parameters.[11] Nevertheless, the variations were mainly observed at the gene expression level. In order to complete this study, in vitro kinetics studies are necessary to clarify cellular pathways involved in coexposure to U and gentamicin.

Acknowledgments

The authors thank C. Baudelin, T. Loiseau, and F. Voyer for their assistance during the animal experiments.

Conflict of interest

The authors declared no conflicts of interest.

Funding

This study was part of the ENVIRHOM research program supported by Institute for Radioprotection and Nuclear Safety (IRSN).

References

1. Domingo JL, Llobet JM, Tomas JM, et al. Acute toxicity of uranium in rats and mice. *Bull Environ Contam Toxicol* 1987; 39(1): 168–174.
2. Zamora ML, Tracy BL, Zielinski JM, et al. Chronic ingestion of uranium in drinking water: a study of kidney bioeffects in humans. *Toxicol Sci* 1998; 43(1): 68–77.
3. Zhu G, Xiang X, Chen X, et al. Renal dysfunction induced by long-term exposure to depleted uranium in rats. *Arch Toxicol* 2009; 83(1): 37–46.
4. Gilman AP, Villeneuve DC, Secours VE, et al. Uranyl nitrate: 28-day and 91-day toxicity studies in the Sprague-Dawley rat. *Toxicol Sci* 1998; 41(1): 117–128.
5. Valko M, Morris H and Cronin MT. Metals, toxicity and oxidative stress. *Curr Med Chem* 2005; 12(10): 1161–1208.
6. Belles M, Linares V, Luisa Albina M, et al. Melatonin reduces uranium-induced nephrotoxicity in rats. *J Pineal Res* 2007; 43(1): 87–95.
7. Pastore A, Federici G, Bertini E, et al. Analysis of glutathione: implication in redox and detoxification. *Clin Chim Acta* 2003; 333(1): 19–39.
8. Lee JM, Li J, Johnson DA, et al. Nrf2, a multi-organ protector? *FASEB J* 2005; 19(9): 1061–1066.
9. Lestaevel P, Romero E, Dhieux B, et al. Different pattern of brain pro-/anti-oxidant activity between depleted and enriched uranium in chronically exposed rats. *Toxicology* 2009; 258(1): 1–9.
10. Linares V, Belles M, Albina ML, et al. Assessment of the pro-oxidant activity of uranium in kidney and testis of rats. *Toxicol Lett* 2006; 167(2): 152–161.
11. Rouas C, Stefani J, Grison S, et al. Effect of nephrotoxic treatment with gentamicin on rats chronically exposed to uranium. *Toxicology* 2011; 279(1-3): 27–35.
12. Silan C, Uzun O, Comunoglu NU, et al. Gentamicin-induced nephrotoxicity in rats ameliorated and healing effects of resveratrol. *Biol Pharm Bull* 2007; 30(1): 79–83.
13. Pedraza-Chaverri J, Gonzalez-Orozco AE, Maldonado PD, et al. Diallyl disulfide ameliorates gentamicin-induced oxidative stress and nephropathy in rats. *Eur J Pharmacol* 2003; 473(1): 71–78.
14. Bennett WM. Mechanisms of aminoglycoside nephrotoxicity. *Clin Exp Pharmacol Physiol* 1989; 16(1): 1–6.
15. Cuzzocrea S, Mazzon E, Dugo L, et al. A role for superoxide in gentamicin-mediated nephropathy in rats. *Eur J Pharmacol* 2002; 450(1): 67–76.
16. Salonen L. 238U series radionuclides as a source of increased radioactivity in groundwater originating from Finnish bedrock. *Future groundwater resources at risk* 1994: 71–84.
17. Diamond GL, Morrow PE, Panner BJ, et al. Reversible uranyl fluoride nephrotoxicity in the Long Evans rat. *Fundam Appl Toxicol* 1989; 13(1): 65–78.
18. Ropenga A, Chapel A, Vandamme M, et al. Use of reference gene expression in rat distal colon after radiation exposure: a caveat. *Radiat Res* 2004; 161(5): 597–602.
19. Itoh M, Oh-Ishi S, Hatao H, et al. Effects of dietary calcium restriction and acute exercise on the antioxidant enzyme system and oxidative stress in rat diaphragm. *Am J Physiol Regul Integr Comp Physiol* 2004; 287(1): R33–38.
20. Chen CF, Tsai SY, Ma MC, et al. Hypoxic preconditioning enhances renal superoxide dismutase levels in rats. *J Physiol* 2003; 552(Pt 2): 561–569.
21. Singh P, Jain A and Kaur G. Impact of hypoglycemia and diabetes on CNS: correlation of mitochondrial oxidative stress with DNA damage. *Mol Cell Biochem* 2004; 260(1-2): 153–159.
22. Leggett RW. The behavior and chemical toxicity of U in the kidney: a reassessment. *Health Phys* 1989; 57(3): 365–383.
23. Priyamvada S, Khan SA, Khan MW, et al. Studies on the protective effect of dietary fish oil on uranyl-nitrate-induced nephrotoxicity and oxidative damage in rat kidney. *Prostaglandins Leukot Essent Fatty Acids* 2010; 82(1): 35–44.
24. Gueguen Y and Rouas C. New data on uranium nephrotoxicity. *Radioprotection* 2012; 47(3): 345–359.
25. Banday AA, Priyamvada S, Farooq N, et al. Effect of uranyl nitrate on enzymes of carbohydrate metabolism and brush border membrane in different kidney tissues. *Food Chem Toxicol* 2008; 46(6): 2080–2088.
26. Taulan M, Paquet F, Argiles A, et al. Comprehensive analysis of the renal transcriptional response to acute uranyl nitrate exposure. *BMC Genomics* 2006; 7: 2.
27. Ghosh S, Kumar A, Pandey BN, et al. Acute exposure of uranyl nitrate causes lipid peroxidation and histopathological damage in brain and bone of Wistar rat. *J Environ Pathol Toxicol Oncol* 2007; 26(4): 255–261.
28. Barber DS, Hancock SK, McNally AM, et al. Neurological effects of acute uranium exposure with and without stress. *Neurotoxicology* 2007; 28(6): 1110–1119.
29. Monleau M, De Meo M, Paquet F, et al. Genotoxic and inflammatory effects of depleted uranium particles inhaled by rats. *Toxicol Sci* 2006; 89(1): 287–295.

30. Brady HR, Kone BC, Brenner RM, et al. Early effects of uranyl nitrate on respiration and K+ transport in rabbit proximal tubule. *Kidney Int* 1989; 36(1): 27–34.
31. Barillet S, Adam C, Palluel O, et al. Bioaccumulation, oxidative stress, and neurotoxicity in Danio rerio exposed to different isotopic compositions of uranium. *Environ Toxicol Chem* 2007; 26(3): 497–505.
32. Gueguen Y, Grandcolas L, Baudelin C, et al. Effect of acetaminophen administration to rats chronically exposed to depleted uranium. *Toxicology* 2007; 229(1-2): 62–72.
33. Tissandie E, Gueguen Y, Lobaccaro JM, et al. Effects of depleted uranium after short-term exposure on vitamin D metabolism in rat. *Arch Toxicol* 2006; 80(8): 473–480.
34. Barouki R. Linking long-term toxicity of xeno-chemicals with short-term biological adaptation. *Biochimie* 2010; 92(9): 1222–1226.
35. Sabath E and Robles-Osorio ML. Renal health and the environment: heavy metal nephrotoxicity. *Nefrologia* 2012; 32(3): 279–286.
36. Shaikh ZA, Vu TT and Zaman K. Oxidative stress as a mechanism of chronic cadmium-induced hepatotoxicity and renal toxicity and protection by antioxidants. *Toxicol Appl Pharmacol* 1999; 154(3): 256–263.
37. Shukla GS, Hussain T, Srivastava RS, et al. Glutathione peroxidase and catalase in liver, kidney, testis and brain regions of rats following cadmium exposure and subsequent withdrawal. *Ind Health* 1989; 27(2): 59–69.
38. Sabolic I. Common mechanisms in nephropathy induced by toxic metals. *Nephron Physiol* 2006; 104(3): p107–114.
39. Djukic-Cosic D, Curcic Jovanovic M, Plamenac Bulat Z, et al. Relation between lipid peroxidation and iron concentration in mouse liver after acute and subacute cadmium intoxication. *Journal of Trace Elements in Medicine and Biology* 2008; 22(1): 66–72.
40. Thijssen S, Cuypers A, Maringwa J, et al. Low cadmium exposure triggers a biphasic oxidative stress response in mice kidneys. *Toxicology* 2007; 236(1-2): 29–41.
41. Liu J, Qu W and Kadiiska MB. Role of oxidative stress in cadmium toxicity and carcinogenesis. *Toxicol Appl Pharmacol* 2009; 238(3): 209–214.
42. Mingeot-Leclercq MP and Tulkens PM. Aminoglycosides: nephrotoxicity. *Antimicrob Agents Chemother* 1999; 43(5): 1003–1112.
43. Maldonado PD, Barrera D, Rivero I, et al. Antioxidant S-allylcysteine prevents gentamicin-induced oxidative stress and renal damage. *Free Radic Biol Med* 2003; 35(3): 317–324.
44. Pedraza-Chaverri J, Maldonado PD, Medina-Campos ON, et al. Garlic ameliorates gentamicin nephrotoxicity: relation to antioxidant enzymes. *Free Radic Biol Med* 2000; 29(7): 602–611.
45. Rouas C, Bensoussan H, Suhard D, et al. Distribution of Soluble Uranium in the Nuclear Cell Compartment at Subtoxic Concentrations. *Chem Res Toxicol* 2010; 23(12): 1883–1889.
46. Abdel-Raheem IT, Abdel-Ghany AA and Mohamed GA. Protective effect of quercetin against gentamicin-induced nephrotoxicity in rats. *Biol Pharm Bull* 2009; 32(1): 61–67.
47. Ozaki N, Matheis KA, Gamber M, et al. Identification of genes involved in gentamicin-induced nephrotoxicity in rats - A toxicogenomic investigation. *Exp Toxicol Pathol* 2009.

Title page including author details

Chronic Uranium Exposure Dose-Dependently Induces Glutathione in Rats without any Nephrotoxicity

Clémentine Poisson (clementine.poisson@irsn.fr) *, Johanna Stefani (johanna.stefani@irsn.fr)*, Line Manens (line.manens@irsn.fr)*, Olivia Delissen (olivia.delissen@irsn.fr)*, David Suhard (david.suhard@irsn.fr)[§], Christine Tessier (christine.tessier@irsn.fr)[§], Isabelle Dublineau (isabelle.dublineau@irsn.fr)[¶], Yann Guéguen (yann.gueguen@irsn.fr)*.

* Institut de Radioprotection et de Sureté Nucléaire (IRSN), PRP-HOM, SRBE, LRTOX, Fontenay-aux-Roses, France. Institut de Radioprotection et de Sureté Nucléaire (IRSN), PRP-HOM, SRBE, LRTOX, Fontenay-aux-Roses, France.

[§] Institut de Radioprotection et de Sureté Nucléaire (IRSN), PRP-HOM, SDI, LRC, Fontenay-aux-Roses, France.

[¶] Institut de Radioprotection et de Sureté Nucléaire (IRSN), PRP-HOM. Fontenay-aux-Roses, France.

Corresponding author: Yann Gueguen

Institut de Radioprotection et de Sûreté Nucléaire (IRSN),

PRP-HOM, SRBE, Laboratoire de RadioToxicologie Expérimentale.

B.P. n°17, 92262

Fontenay-aux-Roses Cedex, FRANCE.

Ph: 33 - 1 58 35 99 78;

Fax: 33 - 1 58 35 84 67

E-Mail: yann.gueguen@irsn.fr

Running title: Chronic uranium exposure induces glutathione.

ACKNOWLEDGMENTS

The authors thank J-M. Guischet,T. Loiseau, and F. Voyer for their assistance during animal's exposure.

Chronic Uranium Exposure Dose-Dependently Induces Glutathione in Rats without any Nephrotoxicity

Running title: Chronic uranium exposure induces glutathione.

ABSTRACT

Uranium (U) is a heavy metal naturally found in the earth's crust that can contaminate the general population when ingested. The acute effect and notably the U nephrotoxicity are well known but knowledge about the effect of chronic U exposure is less clear. In a dose-response study we sought to determine if a chronic exposure to U is toxic to the kidneys and the liver, and what the anti-oxidative system plays in these effects. Rats were contaminated for 3 or 9 months by U in drinking water at different concentrations (0, 1, 40, 120, 400, or 600 mg/L). U accumulation in the liver, kidneys, and bones was linear and proportional to U intake after 3 and 9 months of contamination; it reached 6 $\mu g.g^{-1}$.of kidney tissues for the highest U level in drinking water. Nevertheless, no histological lesions of the kidney were observed, nor any modification of kidney biomarkers such as creatinine or KIM-1. After 9 months of contamination at and above the 120-mg/l concentration of U, lipid peroxidation levels decreased in plasma, liver, and kidneys. Glutathione concentration increased in the liver for the 600-mg/L^{-1} group, in the kidney it increased dose dependently, up to 10-fold, after 9 months of contamination. Conversely, chronic U exposure irregularly modified gene expression and of antioxidant enzymes activities in the liver and kidneys. In conclusion, chronic U exposure did not induce nephrotoxic effects under our experimental conditions, but instead reinforced the anti-oxidant system, especially by increasing glutathione levels in the kidneys.

KEY WORDS: Uranium, chronic exposure, Nephrotoxicity, Oxidative stress, Liver

---

Abbreviations : ANOVA : Analysis of Variance, AU : Arbitrary Units, Ca : Calcium, CAT : Catalase, Cl : Chloride, GADPH : Glyceraldehyde-3-phosphate dehydrogenase, GCS : gamma-Glutamyl Cysteine Synthetase, GGT : Gamma-Glutamyl Transpeptidase, GPx : Glutathione Peroxidase, GR : Glutathione Reductase, GS : Glutathione Synthetase, GSH : Reduced Glutathione, GSSG : Oxidized Glutathione, GST : Glutathione-S-Transferase, HO-1 : Heme Oxygenase 1, HPRT : Hypoxanthine-guanine Phosphoribosyl-Transferase, ICP-MS : Inductively-Coupled Plasma Mass Spectrometry, IRSN : Institut de Radioprotection et de Sureté Nucléaire, K : Potassium, KIM-1 : Kidney Injury Molecule 1, Na : Sodium , NQO1 : NADPH hydrogenase Quinone 1, Nrf2 : Nuclear erythroid factor 2, P : Phosphorus, PCR : Polymerase Chain Reaction, ROS : Reactive Oxygen Species, SGOT : Glutamic-oxaloacetic transaminase, SGPT : glutamic-pyruvic transaminase, SIMS : Secondary Ion Mass Spectrometry, SOD : Superoxide Dismutase, TBARS : Thiobarbituric Acid Reactive Substances, U : Uranium.

1. INTRODUCTION

Uranium (U), like other heavy metals, is dispersed throughout the environment by both natural phenomena and human activities. Consequently humans can be exposed to it. If ingested, two principal organs play a role in its detoxification and elimination: the liver and the kidneys. U accumulates mainly in the kidneys, which are thus the main target of its toxic effects (La Touche et al. 1987; Leggett 1989). Acute exposure to high U levels leads to tubular nephritis and death in rats (Domingo et al. 1987). Only one study has investigated the effect of chronic U exposure after ingestion in a dose-response study: Gilman *et al.* exposed rats to different U concentrations (0.96 to 600 mg/L) for 91 days and observed histological lesions of the renal tubules and glomerules (Gilman et al. 1998). Thus, only sparse data are available, about the mechanisms involved in liver and kidney response to chronic low-level exposure (Berradi et al. 2008; Gueguen et al. 2013; Linares et al. 2006; Taulan et al. 2004).

Oxidative stress, defined as an imbalance between the production of reactive oxygen species (ROS) and the antioxidant system, could explain U toxicity and particularly its nephrotoxicity. This system includes especially enzymes, such as catalase (CAT) and superoxide dismutase (SOD); it also includes glutathione (GSH). The pro-oxidant system, on the other hand, includes reactive species, lipid peroxidation, and carbonylated proteins. Oxidative stress involving a decrease in GSH and an increase in lipid peroxidation in the liver and kidneys has been described after acute U exposure (Yapar et al. 2010). Oxidative stress is also involved in the effects of chronic U exposure in the kidneys, where H_2O_2 increases (Taulan et al. 2004), along with thiobarbituric acid reactive substances (TBARS) and oxidized glutathione (Linares et al. 2006). *In vitro* studies have shown that U contamination of rat hepatocytes leads to an increase in ROS production and a decrease in intracellular glutathione (Pourahmad et al. 2006; Pourahmad et al. 2011). Similarly, ROS production increases in rat kidney cells (NRK-52E) after 20 hours of U exposure at 300 µM (Thiebault et al. 2007).

The aim of this study was i) to determine in a dose-response study if chronic U exposure can induce nephrotoxic or hepatotoxic effects, and ii) to study the pro/antioxidant system and ascertain whether it is related to these effects. Rats were contaminated for 3 or 9 months by U in their drinking water. The U concentrations in this dose-response design ranged from environmental concentrations (1 mg/L) to levels described

by Gilman *et al*. as nephrotoxic (120 and 600 mg/L) (Gilman et al. 1998). The intermediate concentration, 40 mg/L, corresponds to the supra-environmental dose used in our previous studies to investigate several systems and organs (Gueguen et al. 2007; Lestaevel et al. 2009; Racine et al. 2010; Rouas et al. 2011). Chronic exposure for these two different periods —-3 or 9 months — -enabled us to examine whether the organism developed adaptive mechanisms between the two periods. Various biochemical indicators in plasma and urine were measured, and liver and kidney tissue analyzed by histopathological methods. Uranium accumulation in the kidneys, bones, and liver was evaluated by ICP-MS, and its micro distribution in the renal cortex studied with the SIMS technique. Lipid peroxidation in plasma, the liver, and the renal cortex was studied to investigate the pro-oxidant system, while the antioxidant system was assessed in the liver and the renal cortex by examining gene expression of antioxidant enzymes. Finally, glutathione metabolism was studied through the activity of reduced and oxidized glutathione (respectively, GSH and GSSG) and the relevant enzymes, including glutathione peroxidase (GPx), glutathione reductase (GR), and glutathione-S-transferase (GST).

2. MATERIEL & METHODS

2.1 Animals

The study was performed on Sprague Dawley rats provided by Charles River (France). Animals were housed in pairs with a 12-h light/12-h dark cycle and a room temperature of 21 ± 1°C. The study was approved by the IRSN Animal Care Committee and conducted in accordance with French regulations for animal experimentation (Ministry of Agriculture Act No. 2001-464, May 2001).

2.2 Experimental design

2.2.1 Animal exposure to U

Animals were contaminated by drinking water with different U concentrations during 3 (Experiment 1) or 9 (Experiment 2) months. During all 3 months of experiment 1, animals received uranyl nitrate (^{238}U: 99.74%, ^{235}U: 0.26%, ^{234}U 0.001%) (AREVA-NC, France) at four concentrations: 1, 40, 120, or 400 mg/L. During all 9 months of experiment 2, rats received uranyl nitrate (^{238}U: 99%, ^{235}U: 0.76%, ^{234}U: 0.051%) (AREVA-NC, France) at four concentrations: 1, 40, 120, or 600 mg/L. Control animals drank no contaminated water. Each group contained 12 animals.

During the contamination period, food and drink consumption were monitored and the animals weighed weekly.

2.2.2 Tissue, urine, and plasma collection

Animals were anesthetized by inhalation of isoflurane and then euthanized by terminal exsanguination (intracardiac puncture). Both kidneys and the liver were collected and weighed for each rat. The cortex and the medulla of the right kidneys were meticulously separated, flash-frozen in liquid nitrogen, and stored at -80°C. All biological analyses took place in the renal cortex, which is the principal kidney site for U accumulation. Half the left kidney was placed in formaldehyde 4% for histopathological analysis and the other half used for U quantification by ICP-MS and SIMS analyses (the latter used only small volumes, a few mm^3). One lobe of the liver was placed in formaldehyde 4% for histopathological studies, another one for U quantification, and the remaining liver-frozen in liquid nitrogen and stored at -80 °C.

During the contamination period, 24-hour urine samples were collected regularly: every 15 days in experiment 1, and monthly in experiment 2. Animals were placed in metabolic cages 24 hours before the collection began to accustom them at the change of cage. These urine samples were subsequently centrifuged at 3000 g for 10 minutes (4°C). The supernatants were collected and stored at -80°C. Blood was centrifuged at 4000 g for 10 minutes (4°C) to obtain plasma in heparin tubes and serum, all stored at -80°C.

2.2.3 Preparation of samples for SIMS analysis

After euthanasia by terminal exsanguination, small volumes of the renal cortex (a few mm^3) were collected and fixed according to a standard procedure, in a solution containing 6% glutaraldehyde in a sodium cacodylate buffer for 1 day at 48°C, then dehydrated in various ethanol and propylene oxide baths, and permeated with a propylene oxide/Epon mixture (Clerc et al. 1997). The samples were finally embedded in pure Epon-type resin. Serial sections (0.5 µM) embedded in resin were cut and laid on polished ultrapure silicium holders for SIMS analysis or on glass slides for histological examination with a light microscope so that the samples could be observed in their physiological state.

2.2.4 Plasma and urine biochemical indicators

An automated Konelab 20 (ThermoScientific , France) was used to assay urine levels of creatinine, urea, total proteins, uric acid, calcium (Ca), potassium (K), phosphorus (P), chlorine (Cl) and sodium (Na) and plasma levels of , iron, ferritin, transferrin, cholesterol, HDL cholesterol, LDL cholesterol, triglycerides, SGOT (glutamic-oxaloacetic transaminase), SGPT (glutamic-pyruvic transaminase), alkaline phosphatase, direct and total bilirubin, glucose, ceruloplasmin, albumin, urea, uric acid, total proteins, , creatinine, creatine kinase, Ca, K, P, Cl and Na. All the reagents came from Thermo Electron Corporation (France).

2.2.5 Histopathology

The preserved kidney and liver were cut with a microtome, stained with hematoxylin, eosin, and saffron, and examined with a light microscope. An expert laboratory (Biodoxis, France) performed the anatomopathological analyses, scoring tissue from 0 (no damage) to 4 (higher damage). For the kidney histopathological analysis, glomerular damage was defined by the presence of glomerulosclerosis and glomerular

cystic dilatation. Tubular lesions were defined by necrosis, regeneration, dilatation, interstitial inflammation, and interstitial fibrosis. Liver damage was defined by inflammation, necrosis, cytoplasmic vacuolation, and fibrosis.

2.2.6 Secondary ion mass spectrometry (SIMS) microscopy

SIMS microscopy allowed us to analyse the elements and isotopes in solid surfaces by an ion beam coupled with a mass spectrometer. The SIMS analyses were performed with a CAMECA IMS 4F E7 Instrument: $^{40}Ca^{+}$ images provided the histological structure of the kidney and $^{238}U^{+}$ images showed the uranium distribution within it.

2.2.7 ICP-MS

U was quantified in the urine, kidneys, liver, and femur by inductively-coupled plasma mass spectrometry (ICP-MS) (ICP-MS, PQ, Excell, Thermo Electron, France). U was measured in urine after dilution. The organs were digested in nitric acid and hydrogen peroxide and the samples were then evaporated and dissolved in nitric acid. After appropriate dilution, U was measured with bismuth as an internal control and a U calibration range. The detection limit of U was determined by ICP-MS: 0.5 ng/L for ^{238}U and 0.01 ng/L for ^{235}U.

2.2.8 Real Time RT-PCR

Total RNA from the renal cortex was prepared with the RNeasy Total RNA isolation kit (Qiagen, France) according to the manufacturer's instructions. High-capacity cDNA reverse transcription kits (Applied Biosystems Life Technologies, France) were used for the reverse transcription.

Real-time polymerase chain reactions (PCR) were used to analyze the mRNA levels of enzymes involved in the oxidative balance: CAT, manganese, copper, and zinc SOD (Mn, Cu, and Zn SOD), NAD(P)H dehydrogenase Quinone 1 (NQO-1), nuclear factor (erythroid-derived 2)-like 2) (Nrf2), heme oxygenase 1 (HO-1), glutathione synthetase (GS), GSTA1, GR, GPx, gamma-glutamyl-cysteine synthetase (GCS), and gamma-glutamyl transpeptidase (GGT). Table 1 reports the sequences for the forward and reverse primers used in this study. The total volume (10 µL) in each well was adjusted to reach a final concentration

of 1 ng/µL of cDNA, with 83% v/v SYBR (Applied Biosystems, France Life Technologies), 14.5% v/v sterile water, and 2.5% v/v primers (Invitrogen Life Technologies). Optimized PCR used the AbiPrism 7900 Sequence Detection System (Applied Biosystems, France Life Technologies). Samples were normalized to the housekeeping genes, hypoxanthine-guanine phosphoribosyl-transferase (HPRT) and glyceraldehyde-3-phosphate dehydrogenase (GAPDH).The Cycle threshold Ct values of the sample were compared to the geometric average of Ct of both housekeeping genes. Fold induction was calculated relative to the controls. Primer sequences (reverse and forward) are indicated in Table 1 (Chen et al. 2003; Itoh et al. 2004; Poisson et al. 2013; Ropenga et al. 2004; Rouas et al. 2011; Singh et al. 2004; Wierinckx et al. 2005).

2.2.9 Kim-1 assay in urine samples

KIM-1 was evaluated in urine with an ELISA kit used according to the manufacturer's instructions (R&D DY3689 DuoSet, R&D System, France). Urine was diluted to a concentration of 1/10. Results were expressed in pg/nmol of urinary creatinin.

2.2.10 Assays of enzymatic activity and glutathione

For each assay, 25 mg of renal cortex or liver was homogenized in 10 volumes of buffer composed of 50 mM potassium phosphate, pH 6-7, and ethylene diamine tetraacetic acid (EDTA, 1 mM). Tissue samples were then centrifuged at 12 000 g for 10 minutes at 4°C, and the supernatants collected for analyses. Protein concentrations were determined by the Bradford method, with serum albumin as the standard.

GST, GPx, and GR activities were determined with commercial kits supplied by Cayman Chemical (Bertin Pharma, France). GPx activity was assessed indirectly by coupled reaction with glutathione reductase; the oxidized glutathione was recycled to its reduced state by GR and NADPH. NADPH oxidation is accompanied by decreased absorbance at 340 nm directly proportional to GPx activity in the sample. GR was measured by the NADPH oxidation rate. Its oxidation is also accompanied by decreased absorbance at 340 nm, directly proportional to GR activity in the sample. Results were expressed in nmol/min/µg protein. GST activity was evaluated by measuring the conjugation of C-DNB and oxidized glutathione; this results

in increased absorbance at 340 nm, proportional to the GST activity in the sample. The three activities were expressed in nmol/min/µg proteins.

Glutathione, oxidized (GSSG) or reduced (GSH), was assessed with commercial kits supplied by Cayman Chemical in accordance with the manufacturers' instructions.

2.2.11 Lipid peroxidation

Lipid peroxidation was assessed by measuring TBARS, as described by Ohkawa *et al*.(Ohkawa et al. 1979). For measurement in (liver or kidney) tissue, 25 mg of tissue was homogenized in RIPA buffer and centrifuged at 1600 g for 10 minutes at 4°C. Plasma required no preparation. Then, 100 µL of sample or standard was placed in a glass tube and the following ingredients added: 200 µL SDS 8.1% solution. 1.5 mL acetic acid 20%, 1.5 mL TBA 0.8%, and 0.7 ml water. The tubes were then placed in boiling water; at the end of one hour, the reaction was stopped by putting the tubes on ice for 10 minutes. Samples were then extracted by pyridine/butanol by centrifugation at 4000 rpm for 10 minutes at 4°C. Supernatant was collected in triplicate (100 µL each) and read at 530 nm. The results were compared to a range of standard MDA.

2.3. Statistical analysis

A one way analysis of variance (ANOVA) test was used to compare U concentrations in each group.

Two-way ANOVA was used to assess TBARS in plasma, because two variables were considered: time of contamination (3 or 9 months) and U concentration.

All results were expressed as means ± SEM. The level of significance was set at $p<0.05$.

3. RESULTS

3.1 Systemic profile

Body weight and water and food consumption were monitored weekly during the contamination period (data not shown). The U concentration in drinking water did not modify water or food consumption or weight gain: all indicators were similar during both experiments and for each group, including those with the highest (600 mg/L) concentrations. U contamination did not modify rat growth.

3.2 Uranium accumulation and distribution

3.2.1 Accumulation

Uranium (U) accumulation was analyzed by ICP-MS in kidneys and bones (femurs), the target organs of U accumulation, as well as in the liver after 3 and 9 months of U exposure (Figure 1 and Table 2).

Figure 1 represents U accumulation in each of the three tissues after 3 (A) and 9 (B) months of U exposure and shows linear accumulation levels according to the U concentration in the drinking water, regardless of duration of contamination (one-way ANOVA, $p<0.05$). Tissue levels were proportional to the concentration in the drinking water.

Table 2A reports the U quantities measured in the same 3 organs after 3 months of U contamination; these were significantly higher in the groups receiving the highest daily concentrations in that experiment: 120 mg/L and 400 mg/L of U ($p<0.05$). In the kidneys, the U quantity was multiplied by 230 between 1 mg/l group and the (highest) 400 mg/L group. After 9 months of contamination in experiment 2 (Table 2B), the quantity of U in the kidneys, liver, and femur increased from the 40 mg/l group ($p<0.05$); in the group most highly exposed (600 mg/L U), the U concentration in the kidneys exceeded 6 µg per g kidney. The quantity of U in the organs was thus proportional to the U intake.

3.2.2 Distribution

Figure 2 shows the histological view (A) and the superposed images of uranium (red) and calcium (green) ions (B) of proximal tubules in the renal cortex after 9 months of contamination at a U concentration of 120

mg/L. The U distribution in the 600 mg/L group was similar to that in the 120 mg/L group. On image B, the red areas correspond to the U localization, mainly in the proximal tubule cells, but heterogeneous throughout them. This result is consistent with the ICP-MS quantification.

3.3 Histopathology

Figure 3 presents representative microphotographs of lesions observed in rat livers and kidneys at the end of 9 months of U contamination. Two photomicrographs are shown for each organ, for the control and highest-exposure groups. Lesions for the other exposure groups (1, 40, and 120 mg/L) were similar to those in the 600-mg/L group. Moreover, the lesions observed after experiment 1 were similar to those after experiment 2.

U contamination in the liver (Figure 3A) induced no alterations, regardless of the U concentration in the drinking water and of the duration of contamination. Similarly, in figure 3B, the tubular structure of the kidneys was not modified by 3 or 9 months of U contamination. The lesions observed are due to the rats' aging. Similarly, U contamination did not affect the glomerular structure of the kidneys (data not shown).

3.4 Plasma measurements

Table 3 summarizes the representative relevant results for the plasma measurements. Most relevantly, neither kidney function, evaluated by creatinine clearance (which is used to estimate glomerular filtration rate) and urea, nor liver integrity, assessed by SGOT and SGPT, was modified after contamination by any of the U concentrations tested, after either 3 or 9 months.

3.5 Biomarkers of kidney integrity

3.5.1 Traditional biomarkers

Kidney integrity was evaluated by lesion parameters as shown on Figure 4: proteinuria (4A) to estimate glomerular integrity and glycosuria (4B) for tubular integrity. Proteinuria increased significantly from base-line after both 3 and 9 months of contamination for the control group and two contaminated groups (40 and 120 mg/L) ($p<0.05$). This difference is due to the animals' aging. After 3 or 9 months of contamination, neither proteinuria nor glycosuria differed between the control groups and any of the contaminated groups.

3.5.2 Urinary KIM-1 Measurement

KIM-1 is a protein that is overexpressed in tubular cells in cases of kidney impairment. Its early increase in urine is a predictive biomarker of acute or chronic kidney impairment. KIM-1 urinary concentration did not differ between the U-exposed groups and the control groups, regardless of the time of sampling. In experiment 1, comparison of KIM-1 values during the 3 months of contamination shows no variation of KIM-1 as function of time (Fig. 5A). Similarly, in experiment 2, the KIM-1 concentration remained around 90 pmol/nmol of creatinine in every group (Fig. 5B). Other specific and novel biomarkers were evaluated in urine, e.g. clusterin, GST, retinol binding protein, thromboxane B2 and trefoil factor 3 (data not shown) and similar non-significant variations due to U exposure were observed.

3.6 Study of pro/antioxidant equilibrium

3.6.1 Pro-oxidant evaluation: TBARS

Lipid peroxidation was evaluated by measurement of TBARS, corresponding to the MDA (malondialdehyde) concentration.

As Figure 6 shows, plasma TBARS levels were lower in contaminated than control animals after 9 months of U contamination but not after 3 months. The levels in the two control groups did not differ. After 9 months, the TBARS level was lower in every exposed group, but significantly so for only the two highest exposure (120 and 600 mg/L) groups ($p<0.05$). Comparison between animals after 3 and 9 months of U contamination indicates a significant decrease in TBARS levels only for the group of rats exposed to 120 mg/l of U for 9 months ($p<0.05$). This result suggests that animal aging combined with U exposure might influence these levels in plasma. Globally the plasma MDA concentration after 9 months of contamination was lower than after 3 months of contamination, albeit not significantly.

Figure 7 presents the TBARS levels in liver and kidney tissue after 9 months. In the liver, U contamination appeared to induce a non-significant decrease in lipid peroxidation in all but the lowest exposure group. In the kidney tissue, TBARS levels also decreased, and the different was significant for the two highest exposure groups: 120 mg/L ($p<0.05$) and 600 mg/l ($p<0.01$) groups.

3.6.2 Glutathione Metabolism after 3 Months of U Contamination

After 3 months of exposure, liver levels of GSH and GSSG in the exposed rats did not differ significantly from those in the control group (Figure 8A). Similarly the activities of the three antioxidant enzymes (GPx, GR, and GST) did not vary.

In the renal cortex (Figure 8B), on the other hand, the GSH level increased significantly for the highest U concentration ($p<0.05$), but the GSSG level was not significantly different between the control group and any of the exposed groups. The same was true for GR activity. GPx activity increased significantly but only for the 40 mg/l group. GST activity decreased significantly for the three lowest U concentrations: 1, 40, and 120 mg/L ($p<0.05$).

3.6.3 Glutathione Metabolism after 9 Months of U contamination

In experiment 2, as Figure 9A shows, the GSH level in the liver increased only for the rats exposed to the highest U level (600 mg/L) (x1.3, $p<0.05$), but the oxidized form did not differ between the control group and any of the exposed groups. Nine months of U exposure did not affect the activities of the two antioxidant enzymes – GPx and GR — in the liver either, but GST activity decreased for the highest U concentrations (120 and 600 mg/L).

Analyses of the renal cortex in experiment 2 (Figure 9B) showed that the GSH level increased after U contamination for all but the lowest concentration ($p<0.001$): it was five times higher in the 40 mg/l group compared with the control group, 8.6 times higher for the 120 mg/L group, and 10 times for the highest concentration. The significant increase between each group (data not shown, $p<0.001$) showed a dose effect response. The GSSG level did not differ between the control group and any of the exposed groups, nor did GPx, GR, or GST activities.

3.6.4 Gene Expression of Different Enzymes and Transcription Factors Involved in Oxidative Stress

Gene expression of antioxidant enzymes or transcription factors was evaluated by PCR in the liver (Figure 10) and kidneys (Figure 11) after 3 and 9 months of U contamination. The mRNA level of its transcription

factor was used to evaluate Nrf2. Finally, the following antioxidant enzymes were evaluated: Mn,Cu, and Zn SOD, CAT, GR, GPx, GSTa1, GCS, GGT, GS, HO 1, and NQO1.

U contamination did not modify gene expression of the antioxidant genes in the liver (Figure 10) after 3 or 9 months at any tested concentration. A decrease was observed for GPx and GSTa2 after 3 months of uranium contamination in the 1-mg/l group (-39% and -27% respectively, $p<0.05$). Gene expression of Cu, Zn SOD after 9 months of contamination decreased for the 40 mg/L group (-25%, $p<0.05$). Gene expression of GR and GS also decreased significantly in all but the lowest concentration group after 9 months of contamination (-25%, $p<0.05$).

Sporadic modifications of gene expression were observed in the renal cortex (Figure 11). After 3 months of U contamination, gene expression of GS decreased in the highest dose group (-44%, $p<0.05$). HO 1 gene expression decreased for the 40 mg/L group (-36%, $p<0.05$). CAT gene expression increased after 3 months of U contamination for the 400 mg/L group (20%, $p<0.05$). After 9 months of contamination, the only antioxidant factor investigated that U modified was HO 1. In the highest dose group, expression of the HO 1 gene decreased (-36%, $p<0.05$).

4. DISCUSSION

U accumulated in rat bones and kidneys linearly and proportionally, without any plateau in this dose-response study in which rats were contaminated for two separate long periods (3 and 9 months) with different concentrations of U in their drinking water (0 to 600 mg/L, corresponding to a calculated body burden of 0 to 40 mg/kg/day) (Table 2). Our aim was to determine whether chronic U exposure induces nephrotoxic effects or disrupts the pro/antioxidant system in the liver and kidneys. Gilman *et al*. described this effect in rat kidneys, but only during 91 days of contamination (Gilman et al. 1998), by ingestion of 0.02 mg/kg/day to 40 mg/kg/day. They reported the nephrotoxic U threshold to be 0.4 µg/g of kidney, much lower than generally accepted in the literature —3 µg/g of kidney (ATSDR 2013). In our work, the quantity of U found in kidney tissue after 9 months of contamination was around 6 µg/g of kidney for the highest U concentration (600 mg/L), and neither the histological nor the biomarker analyses showed any toxic effects. We also found, as many others have reported, that substantially higher quantities of U accumulated in the kidneys and bones than in the liver (Gilman et al. 1998; Paquet et al. 2006; Zhu et al. 2009a).

The study of U microdistribution shows that at body doses of 2.67 to 40 mg/kg/day U is found mainly in the nucleus of proximal tubular cells and to a lesser extent in other renal structures (Figure 2). Tessier *et al.* previously reported that U is preferentially distributed in proximal tubular cells through 9 months of exposure (Tessier et al. 2012), but that after 12 or 18 months of contamination, accumulation becomes more heterogeneous, with U also found in other renal structures, including the glomeruli or distal convoluted tubules. Furthermore, our dose-response study with the SIMS technique shows that U presence in proximal tubular cells is more elevated at the higher concentrations than in the other groups, in accordance with the ICP-MS measurements.

Many studies of acute exposure have determined that U accumulation in rat kidneys causes nephrotoxic effects based on changes in biomarker levels, such as increasing plasma creatinine and urea, and histological modifications in the proximal tubules (Diamond et al. 1989; Domingo et al. 1987; Sun et al. 2002; Taulan et al. 2006; Zimmerman et al. 2007). Few studies of chronic exposure, however, have demonstrated modifications in biomarkers. Zhu *et al.* reported an increase in plasma urea and creatinine and an increase in urinary $ß_2$-microglobulin after 3 to 12 months of U treatment of rats by implants (200 to 600

mg/kg) (Zhu et al. 2009b).These differences from our results can be explained by the different exposure conditions (implant *versus* oral route) or doses (up to 35 µg U per gram of kidney in Zhu's study). Our study regularly monitored kidney integrity and function by testing urine levels of creatinine, urea, and KIM-1, a specific biomarker of tubular integrity. Under our experimental conditions, chronic contamination did not induce any modification of these renal indicators. A previous study assessed KIM-1 at the end of 9 months of chronic U exposure but only at a single U concentration (2.67 mg/kg/day) and in a study where the rats were also treated with gentamicin, a nephrotoxic antibiotic, during the last week of contamination (Rouas et al. 2011). The chronic exposure did not aggravate the increase in KIM-1 due to the gentamicin.

Simultaneously, histological analyses of the kidney and liver confirmed the absence of any difference between the U-contaminated groups for lesions of kidney and liver tissue. This finding is correlated to the absence of any modifications in transaminase levels in the liver integrity evaluation. Conversely, other studies of chronic exposure have shown histological changes in rat kidneys, including the formation of vacuoles in TCP and glomerular alterations (Gilman et al. 1998; Zhu et al. 2009b) observed from the lowest concentration upward in Gilman's study.

These results led us to conclude that after chronic exposure U accumulates linearly in the liver, kidneys, and bones, and has a specific distribution in the kidneys, but does not induce nephrotoxic effects after chronic exposure, regardless of the U concentration. As we pointed out above, the threshold toxicity for acute U exposure is reported to be 3 µg/g of kidney tissue, but in our experimental conditions of chronic exposure, U accumulation reached 6 µg/g of kidney at maximum without any nephrotoxic effects observed.

This lack of toxicity after chronic exposure may result from a defense or adaptive mechanism that organisms may develop against toxic substances. One such mechanism is the antioxidant system, which is reported to be activated after exposure to other heavy metals, including cadmium and lead (Sabath and Robles-Osorio 2012; Sabolic 2006). Some authors have thus investigated the role of oxidative stress in the U-induced effects of chronic exposure. Linares *et al.* contaminated rats through U in their drinking water (10, 20 and 40 mg/kg/day) and observed an increase in renal lipid peroxidation for the highest concentration. Similarly, chronic U exposure of mice (4 months, 13 to 26 mg/kg/day) produced an increase in

lipid peroxidation (Taulan et al. 2004). Conversely, in our study, as Figure 7B shows, lipid peroxidation in the kidney decreased and GSH increased dose dependently after 9 months of contamination (Figure 9B).

No previous studies of which we are aware studied oxidative stress in the liver after chronic U exposure. On the other hand, acute exposure in mice (5 mg/kg of body weight by oral gavage for 5 days) decreased glutathione levels and significantly increased MDA levels (Yapar et al. 2010). Our results showed that U contamination induced a decrease in TBARS levels (Figure 7A) and an increase in GSH and GST activity in the liver after 9 months in the groups with the highest U concentrations (120 mg/L and 600 mg/L, corresponding to 8 mg/kg and 40 mg/kg), whereas GR and GPx activities were not modified (Figure 9A).

Globally, an increase in the pro-oxidant system in response to oxidative stress is generally reported to increase TBARS levels and decrease glutathione levels and the functioning of the antioxidant system (Linares et al. 2006; Periyakaruppan et al. 2007; Yapar et al. 2010). Surprisingly, we found here that U contamination appeared to reinforce the antioxidant system, especially the glutathione pool. The organism reacted by implementing a compensatory mechanism that seems to prevent the adverse effects of U contamination. This increase in GSH has also been observed in kidneys after 45 days of cadmium exposure (Mendieta-Wejebe et al. 2013). Those authors hypothesized that the organism set compensatory mechanisms in action, explaining that the increase in glutathione counters the excessive ROS production and protects the membrane from attack by hydroxyl radicals ($HO^{\cdot}$). These mechanisms might also be put into place after chronic U contamination.

The antioxidant system was functional and reactive in our study, consistent with the results of previous studies of detoxification systems in our laboratory (Gueguen et al. 2007; Gueguen et al. 2013; Poisson et al. 2013; Rouas et al. 2011). Those studies have examined other defense mechanisms in rats, such as xenobiotic metabolism enzymes in case of co-exposure by U and a drug. For example, co-treatment by chronic U exposure (2.67 mg/kg/day, 9 months) and acute nephrotoxic gentamicin treatment during the last week of contamination did not potentiate or inhibit the effect of gentamicin on either defense system: XME or the antioxidant system (Poisson et al. 2013; Rouas et al. 2011).

Overall, this study is the first to test chronic U exposure with concentrations up to 600 mg/L or 40 mg/kg/day (6 µg/g of kidney), and we did not observe any nephrotoxicity. Our results confirm that chronic

exposure to U is different from the addition of several acute U exposures, a finding consistent with those for other heavy metals (Liu et al. 2009). Chronic U exposure appears to reinforce the antioxidant system. Nevertheless, it does disrupt the pro/antioxidant system, especially glutathione homeostasis. This finding suggests that glutathione may play a key role in regulation of oxidative stress in cases of chronic U exposure.

5. FUNDING INFORMATION

This work was supported by Institute for Radioprotection and Nuclear Safety (IRSN). This study was part of the ENVIRHOM research program of the IRSN.

6. CONFLICT OF INTEREST

The authors declared no conflicts of interest.

BIBLIOGRAPHY

ATSDR. 2013. Toxicological Profile for Uranium Public health service Atlanta

Berradi, H., Bertho, J.M., Dudoignon, N., Mazur, A., Grandcolas, L., Baudelin, C., Grison, S., Voisin, P., Gourmelon, P. and Dublineau, I. 2008. Renal anemia induced by chronic ingestion of depleted uranium in rats. Toxicol Sci 103, 397-408.

Chen, C.F., Tsai, S.Y., Ma, M.C. and Wu, M.S. 2003. Hypoxic preconditioning enhances renal superoxide dismutase levels in rats. J Physiol 552, 561-569.

Clerc, J., Fourre, C. and Fragu, P. 1997. SIMS microscopy: methodology, problems and perspectives in mapping drugs and nuclear medicine compounds. Cell biology international 21, 619-633.

Diamond, G.L., Morrow, P.E., Panner, B.J., Gelein, R.M. and Baggs, R.B. 1989. Reversible uranyl fluoride nephrotoxicity in the Long Evans rat. Fundam Appl Toxicol 13, 65-78.

Domingo, J.L., Llobet, J.M., Tomas, J.M. and Corbella, J. 1987. Acute toxicity of uranium in rats and mice. Bull Environ Contam Toxicol 39, 168-174.

Gilman, A.P., Villeneuve, D.C., Secours, V.E., Yagminas, A.P., Tracy, B.L., Quinn, J.M., Valli, V.E., Willes, R.J. and Moss, M.A. 1998. Uranyl nitrate: 28-day and 91-day toxicity studies in the Sprague-Dawley rat. Toxicol Sci 41, 117-128.

Gueguen, Y., Grandcolas, L., Baudelin, C., Grison, S., Tissandie, E., Jourdain, J.R., Paquet, F., Voisin, P., Aigueperse, J., Gourmelon, P. and Souidi, M. 2007. Effect of acetaminophen administration to rats chronically exposed to depleted uranium. Toxicology 229, 62-72.

Gueguen, Y., Rouas, C., Monin, A., Manens, L., Stefani, J., Delissen, O., Grison, S. and Dublineau, I. 2013. Molecular, cellular, and tissue impact of depleted uranium on xenobiotic-metabolizing enzymes. Arch Toxicol.

Itoh, M., Oh-Ishi, S., Hatao, H., Leeuwenburgh, C., Selman, C., Ohno, H., Kizaki, T., Nakamura, H. and Matsuoka, T. 2004. Effects of dietary calcium restriction and acute exercise on the antioxidant enzyme system and oxidative stress in rat diaphragm. American journal of physiology. Regulatory, integrative and comparative physiology 287, R33-38.

La Touche, Y.D., Willis, D.L. and Dawydiak, O.I. 1987. Absorption and biokinetics of U in rats following an oral administration of uranyl nitrate solution. Health Phys 53, 147-162.

Leggett, R.W. 1989. The behavior and chemical toxicity of U in the kidney: a reassessment. Health Phys 57, 365-383.

Lestaevel, P., Romero, E., Dhieux, B., Ben Soussan, H., Berradi, H., Dublineau, I., Voisin, P. and Gourmelon, P. 2009. Different pattern of brain pro-/anti-oxidant activity between depleted and enriched uranium in chronically exposed rats. Toxicology 258, 1-9.

Linares, V., Belles, M., Albina, M.L., Sirvent, J.J., Sanchez, D.J. and Domingo, J.L. 2006. Assessment of the pro-oxidant activity of uranium in kidney and testis of rats. Toxicol Lett 167, 152-161.

Liu, J., Qu, W. and Kadiiska, M.B. 2009. Role of oxidative stress in cadmium toxicity and carcinogenesis. Toxicol Appl Pharmacol 238, 209-214.

Mendieta-Wejebe, J.E., Miliar-Garcia, A., Correa-Basurto, J., Sanchez-Rico, C., Ramirez-Rosales, D., Trujillo-Ferrara, J. and Rosales-Hernandez, M.C. 2013. Comparison of the effect of chronic cadmium exposure on the antioxidant defense systems of kidney and brain in rat. Toxicology mechanisms and methods 23, 329-336.

Ohkawa, H., Ohishi, N. and Yagi, K. 1979. Assay for lipid peroxides in animal tissues by thiobarbituric acid reaction. Anal Biochem 95, 351-358.

Paquet, F., Houpert, P., Blanchardon, E., Delissen, O., Maubert, C., Dhieux, B., Moreels, A.M., Frelon, S. and Gourmelon, P. 2006. Accumulation and distribution of uranium in rats after chronic exposure by ingestion. Health Phys 90, 139-147.

Periyakaruppan, A., Kumar, F., Sarkar, S., Sharma, C.S. and Ramesh, G.T. 2007. Uranium induces oxidative stress in lung epithelial cells. Arch Toxicol 81, 389-395.

Poisson, C., Rouas, C., Manens, L., Dublineau, I. and Gueguen, Y. 2013. Antioxidant status in rat kidneys after coexposure to uranium and gentamicin. Human & experimental toxicology.

Pourahmad, J., Ghashang, M., Ettehadi, H.A. and Ghalandari, R. 2006. A search for cellular and molecular mechanisms involved in depleted uranium (DU) toxicity. Environ Toxicol 21, 349-354.

Pourahmad, J., Shaki, F., Tanbakosazan, F., Ghalandari, R., Ettehadi, H.A. and Dahaghin, E. 2011. Protective effects of fungal beta-(1-->3)-D-glucan against oxidative stress cytotoxicity induced by depleted uranium in isolated rat hepatocytes. Hum Exp Toxicol 30, 173-181.

Racine, R., Grandcolas, L., Blanchardon, E., Gourmelon, P., Veyssiere, G. and Souidi, M. 2010. Hepatic cholesterol metabolism following a chronic ingestion of cesium-137 starting at fetal stage in rats. J Radiat Res 51, 37-45.

Ropenga, A., Chapel, A., Vandamme, M. and Griffiths, N.M. 2004. Use of reference gene expression in rat distal colon after radiation exposure: a caveat. Radiat Res 161, 597-602.

Rouas, C., Stefani, J., Grison, S., Grandcolas, L., Baudelin, C., Dublineau, I., Pallardy, M. and Gueguen, Y. 2011. Effect of nephrotoxic treatment with gentamicin on rats chronically exposed to uranium. Toxicology 279, 27-35.

Sabath, E. and Robles-Osorio, M.L. 2012. Renal health and the environment: heavy metal nephrotoxicity. Nefrologia : publicacion oficial de la Sociedad Espanola Nefrologia 32, 279-286.

Sabolic, I. 2006. Common mechanisms in nephropathy induced by toxic metals. Nephron Physiol 104, p107-114.

Singh, P., Jain, A. and Kaur, G. 2004. Impact of hypoglycemia and diabetes on CNS: correlation of mitochondrial oxidative stress with DNA damage. Mol Cell Biochem 260, 153-159.

Sun, D.F., Fujigaki, Y., Fujimoto, T., Goto, T., Yonemura, K. and Hishida, A. 2002. Relation of distal nephron changes to proximal tubular damage in uranyl acetate-induced acute renal failure in rats. Am J Nephrol 22, 405-416.

Taulan, M., Paquet, F., Argiles, A., Demaille, J. and Romey, M.C. 2006. Comprehensive analysis of the renal transcriptional response to acute uranyl nitrate exposure. BMC Genomics 7, 2.

Taulan, M., Paquet, F., Maubert, C., Delissen, O., Demaille, J. and Romey, M.C. 2004. Renal toxicogenomic response to chronic uranyl nitrate insult in mice. Environ Health Perspect 112, 1628-1635.

Tessier, C., Suhard, D., Rebiere, F., Souidi, M., Dublineau, I. and Agarande, M. 2012. Uranium microdistribution in renal cortex of rats after chronic exposure: a study by secondary ion mass spectrometry microscopy. Microsc Microanal 18, 123-133.

Thiebault, C., Carriere, M., Milgram, S., Simon, A., Avoscan, L. and Gouget, B. 2007. Uranium induces apoptosis and is genotoxic to normal rat kidney (NRK-52E) proximal cells. Toxicol Sci 98, 479-487.

Wierinckx, A., Breve, J., Mercier, D., Schultzberg, M., Drukarch, B. and Van Dam, A.M. 2005. Detoxication enzyme inducers modify cytokine production in rat mixed glial cells. J Neuroimmunol 166, 132-143.

Yapar, K., Cavusoglu, K., Oruc, E. and Yalcin, E. 2010. Protective role of Ginkgo biloba against hepatotoxicity and nephrotoxicity in uranium-treated mice. J Med Food 13, 179-188.

Zhu, G., Tan, M., Li, Y., Xiang, X., Hu, H. and Zhao, S. 2009a. Accumulation and distribution of uranium in rats after implantation with depleted uranium fragments. J Radiat Res (Tokyo) 50, 183-192.

Zhu, G., Xiang, X., Chen, X., Wang, L., Hu, H. and Weng, S. 2009b. Renal dysfunction induced by long-term exposure to depleted uranium in rats. Arch Toxicol 83, 37-46.

Zimmerman, K.L., Barber, D.S., Ehrich, M.F., Tobias, L., Hancock, S., Hinckley, J., Binder, E.M. and Jortner, B.S. 2007. Temporal clinical chemistry and microscopic renal effects following acute uranyl acetate exposure. Toxicol Pathol 35, 1000-1009.

FIGURE LEGENDS

Figure 1: Uranium accumulation in liver (♦),bone femur (■) and kidney (●) after 3 (A) or 9 (B) months of contamination .

Part A, n=6 per group. Part B n=12 per group. Asterisks indicate a significant difference between the contaminated and control groups (1, 40, 120, 400, or 600 mg/l) (one-way ANOVA, $p<0.05$).

Figure 2: Representative histological view (A) and superposed ionic images (B) of uranium (red) and calcium (green) of proximal tubules in the renal cortex after 9 months of contamination by uranium in their drinking water(120 mg/L) (field 200 x 200 µm)

Figure 3: Representative microphotographs of liver (A) or renal (B) tissue in rats at the end of 9 months of contamination by uranium in their drinking water.

Microphotograph A1 shows mild periportal and intra-lobular biliary hyperplasia, minimal peribiliary fibrosis, and inflammation. Microphotograph A2 shows minimal biliary duct hyperplasia, minimal fibrosis, and inflammation. Microphotograph B1 shows tubular regeneration, tubular dilatation, fibrosis, and inflammation,

while microphotograph B2 shows tubular regeneration, focal glomerulosclerosis, fibrosis, and inflammation.

Figure 4: Urine levels of proteins (A) and glucose (B)after 3 or 9-month chronic exposure of rats to uranium (U) in drinking water. Control ■ 1 mg/L ■ 40 mg/L ■ 120 mg/L ■ 400-600 mg/L

The concentration of U in drinking water was from 1 to 400 mg/L during the 3-month-experiment (full bar) and 1 to 600 mg/L during the 9-month experiment (hashed bar). Results are expressed as the mean ± SEM. The hash indicates a significant difference between 3 and 9 months (two-way ANOVA, # $p<0.05$, ## $p<0.01$, ### $p<0.001$,).

Figure 5: Monitoring of tubular integrity: KIM 1 measurement during 3 (A) and 9 (B) months of contamination of rats by uranium in drinking water. Control ■ 1 mg/L ■ 40 mg/L ■ 120 mg/L ■ 400-600 mg/L

KIM-1 was evaluated every 2 weeks in experiment 1 (A) and monthly in experiment 2 (B). The concentration of U in drinking water was 1-400 mg/L during the 3-month experiment and 1-600 mg/L during the 9-month experiment. . The results are expressed as the mean ± SEM.

Figure 6: TBARS levels in plasma after 3 and 9 months of contamination of rats by uranium in their drinking water. Control ■ 1 mg/L ■ 40 mg/L ■ 120 mg/L ■ 400-600 mg/L

TBARS levels correspond to MDA concentrations (µmol/l). The concentration of U in drinking water was from 1 to 400 mg/L during the 3-month experiment (full bar) and 1 to 600 mg/L during the 9-month experiment (hashed bar). The hash indicates a significant difference between 3 and 9 months (two-way ANOVA, $p<0.05$), and the asterisk a significant difference between the contaminated and control rats (one-way ANOVA, *$p<0.05$, **$p<0.01$, ***$p<0.01$).

Figure 7: TBARS levels in liver (A) and kidney (B) tissue after 9 months of contamination of rats by uranium in their drinking water. Control ■ 1 mg/L ■ 40 mg/L ■ 120 mg/L ■ 400-600 mg/L

TBARS levels correspond to MDA in µmol per mg of protein. Asterisks indicate a significant difference between the contaminated and control rats (one-way ANOVA, *p<0.05, **p<0.01, ***p<0.01).

Figure 8: Glutathione metabolism in liver (A) and kidney (B) tissue after 3 months of contamination of rats by uranium in their drinking water. Control ■ 1 mg/L ■ 40 mg/L ■ 120 mg/L ■ 400-600 mg/L

Glutathione homeostasis after 3 months of uranium contamination was evaluated by the concentration of GSH and GSSG, and the activity of GPx, GR, and GST for control and contaminated rats (n=12 for each group). The results are expressed in nanomole per minute per mg of protein. Asterisks indicate a significant difference between the contaminated and control rats (one-way ANOVA, *p<0.05, **p<0.01, ***p<0.01). GSH: reduced glutathione, GSSG: oxidized glutathione, GPx glutathione peroxidase:, GR: glutathione reductase, GPx: glutathione peroxidase, GST: glutathione-S-transferase.

Figure 9: Glutathione metabolism in liver (A) and kidney (B) tissue after 9 months of contamination of rats by uranium in their drinking water. Control ■ 1 mg/L ■ 40 mg/L ■ 120 mg/L ■ 400-600 mg/L

Glutathione homeostasis after 9 months of uranium contamination was evaluated by the concentration of GSH and GSSG, and the activity of GPx, GR, and GST for control and contaminated rats (n=12 for each group). The results are expressed in nanomole per minute per mg of protein. Asterisks indicate a significant difference between the contaminated and control rats (one-way ANOVA, *p<0.05, **p<0.01, ***p<0.01). GSH: reduced glutathione, GSSG: oxidized glutathione, GPx glutathione peroxidase:, GR: glutathione reductase, GPx: glutathione peroxidase, GST: glutathione-S-transferase.

Figure 10: Gene expression in liver tissue after 3 (A) or 9 (B) months of contamination of rats by uranium in their drinking waterThe ratio is expressed as a ratio of the mRNA levels of the geometric mean of two housekeeping genes (hypoxanthine-guanine phosphoribosyl transferase and glyceraldehyde 3-phosphate dehydrogenase). The concentration of U in drinking water was 1-400 mg/L during the 3-month experiment and 1-600 mg/L during the 9-month experiment.. Asterisks indicate a significant difference between the contaminated and control rats (one-way ANOVA, * p<0.05).

Figure 11: Gene expression in kidney after 3 (A) or 9 (B) months of uranium contamination in non-exposed and contaminated rats

The ratio is expressed as a ratio of the mRNA levels of the geometric mean of two housekeeping genes (hypoxanthine-guanine phosphoribosyl transferase and glyceraldehyde 3-phosphate dehydrogenase). The concentration of U in drinking water was 1-400 mg/L during the 3-month experiment and 1-600 mg/L during the 9-month experiment. Asterisks indicate a significant difference between the contaminated and control rats (one-way ANOVA, * $p<0.05$).

Table
Click here to download Table: Tables .docx

TABLES

Table 1. Primer sequences for genes encoding antioxidant enzymes

(HPRT: hypoxanthine-guanine phosphoribosyl-transferase, GAPDH: Glyceraldehyde-3-phosphate dehydrogenase, Cu, Zn SOD: Copper, Zinc Superoxide Dismutase, GCS: Gamma glutamyl cysteine synthetase, GGT: Gamma-glutamyl-transpeptidase, GPx: Glutathione peroxidase, GR: Glutathione reductase, GS: Glutathione synthetase, GSTA2: Glutathione-S-transferase A2, HO-1: Heme oxygenase 1, Mn SOD : Manganese superoxide dismutase, NQO1: NAD(P)H dehydrogenase Quinone 1, Nrf2: Nuclear factor (erythroid-derived 2)-like 2).

Gene	Forward	Reverse	Reference
HPRT	GCT CGA GAT GTC ATG AAG GAG A	TCA GCG CTT TAA TGT AAT CCA GC	Ropenga et al. 2004
GAPDH	GGC CAA GGT CAT CCA TGA	TCA GTG TAG CCC AGG ATG	This study
CAT	GAG AGG AAA CGC CTG TGT GAG	AAG AGC CTG GAC TCG GGC CC	Singh, 2004
Cu, Zn SOD	GAT TAA CTG AAG GCG AGC AT	CCG CCA TGT TTC TTA GAG T	Itoh, 2004
GCS	GGA ACG ATG TCC GAG TTC AA	GTT ATC GTG CAA AGA GCC TGA T	This study
GGT	AGA GCC TTG GAC AAA AAA CGG	TGC AAC GTA TCG GCC AAC T	This study
GPx	TGC AAT CAG TTC GGA CAT CA	ACC ATT CAC CTC GCA CTT C	Itoh, 2004
GR	TTG CTG GCC TCT ATT CAC TGG	ATT ACC TCC GCC CTC TCT TTG	Poisson, 2013
GS	TTG CTG GCC TCT ATT CAC TGG	ATT ACC TCC GCC CTC TCT TTG	Poisson, 2013
GSTA2	TTG ACA TGT ATT CAG AGG GT	TTG TTT TGC ATC CAT GGC TG	Rouas, 2009
HO-1	ATG CCC CAC TCT ACT TCC CTG A	TGC TGT GTG GCT GGT GTG TAA G	Poisson, 2013
Mn SOD	ACG CGA CCT ACG TGA ACA ATCT	CAG TGC AGG CTG AAG AGC AA	Chen, 2003
NQO1	AACGTCATTCTCTGGCCAATTC	GCCAATGCTGTACACCAGTTGA	Wierinckx, 2005
Nrf2	TGG GTT CAG TGA CTC GGA AAT	TGG CTG TGC TTT AGG TCC ATT	This study

Table 2: Uranium Quantification in the Liver, Femur and Kidneys after 3 (A) and 9 (B) months of uranium contamination

Uranium concentration was evaluated in the tissue by ICP-MS and expressed in ng/g tissue. The values are expressed as mean± SEM. Part A, n=6 per group. Part B n=12 per group. Asterisks correspond to a significant difference between control and contaminated group (1, 40, 120, 400 or 600 mg/L) (one-way ANOVA, * $p<0.05$). The symbol $ represents a significant difference between the 600 mg/L group and the other contaminated group and the symbol ¤ between the 120 mg/L group and the other contaminated groups (one-way ANOVA, $, ¤ $p<0.05$).

A) 3 months Uranium concentration in drinking water intake (mg/L)	Uranium quantity (ng/g tissue) (mean ± SEM)		
	Liver	Femur	Kidney
0	0.34 ± 0.02	7.3 ± 1.7	7.1 ± 1
1	0.63 ± 0.2 $	7.5 ± 0.3 $	11.6 ± 1.1 $
40	1.21 ± 0.1	61 ± 5.5	208 ± 10.8
120	3.45 ± 0.3*	386 ± 24 *	1056 ± 185*
400	7 ± 0.63 *	987 ± 72 *	2669 ± 362 *
B) 9 months Uranium concentration in drinking water intake (mg/L)	Uranium quantity (ng/g tissue) (mean ± SEM)		
	Liver	Femur	Kidney
0	0.16 ± 0.02	6.99 ± 0.8	6.6 ± 1.09
1	0.2 ± 0.02 $ ¤	9.99 ± 0.85 $	12.9 ± 1.3 $ ¤
40	1.9 ± 0.6 *	176 ± 19.1 *	217 ± 34.7* $
120	3.6 ± 0.2 *	525 ± 39 *	1038 ± 246 * $
600	24 ± 1.9 *	2626 ± 342 *	6132± 768 *

Table 3: Plasma Indicators After 3 or 9 Months of Uranium Contamination (n=12 for each group).

Exposure time	**3 Months**				
Plasma Indicators	Uranium concentration (mg/L)				
	0	1	40	120	400
Urea (mM)	6 ± 0.19	6 ± 0.21	5.7 ± 0.13	5.95 ± 0.2	5.8 ± 0.14
Creatinine clearance (ml/min/kg)	4 ± 0.2	4.4 ± 0.33	4.5 ± 0.1	3.4 ± 0.4	4 ± 0.1
TGO (U/l)	137 ± 13	169 ± 31.6	128.5 ± 15.6	137 ± 17.5	180.4 ± 24.6
TGP(U/:)	49.9 ± 3.8	65.5 ± 9.7	57.8 ± 9.8	61.4 ± 9.6	61.8 ± 10.9
Exposure time	**9 Months**				
Plasma Indicators	Uranium concentration (mg/L)				
	0	1	40	120	600
Urea (mM)	6.15 ± 0.2	5.9 ± 0.2	6.44 ± 0.3	6.15 ± 0.2	6.1 ± 0.22
Creatinine clearance (mL/min/kg)	3.4 ± 0.2	3.5 ± 0.3	2.9 ± 0.14	3.3 ± 0.94	3.3 ± 0.16
TGO (U/l)	185 ± 16.7	212 ± 44	193 ± 37	202.6 ± 32	176.7 ± 22.6
TGP(U/l)	39.8 ± 3	54 ± 7.7	48.9 ± 6.3	58.9 ± 8.6	48.6 ± 8

Figure 1

Click here to download Figure: Figure 1.pptx

Figure 1

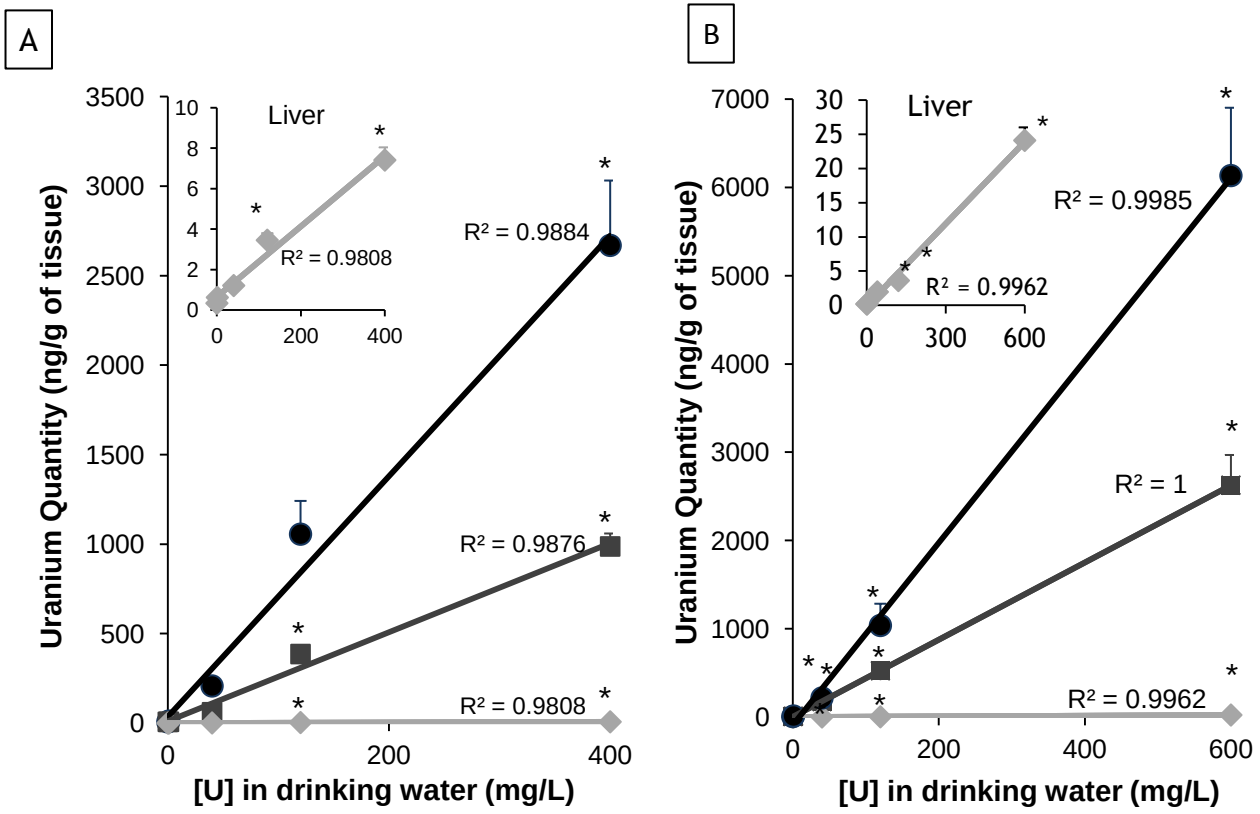

Figure 2

Click here to download high resolution image

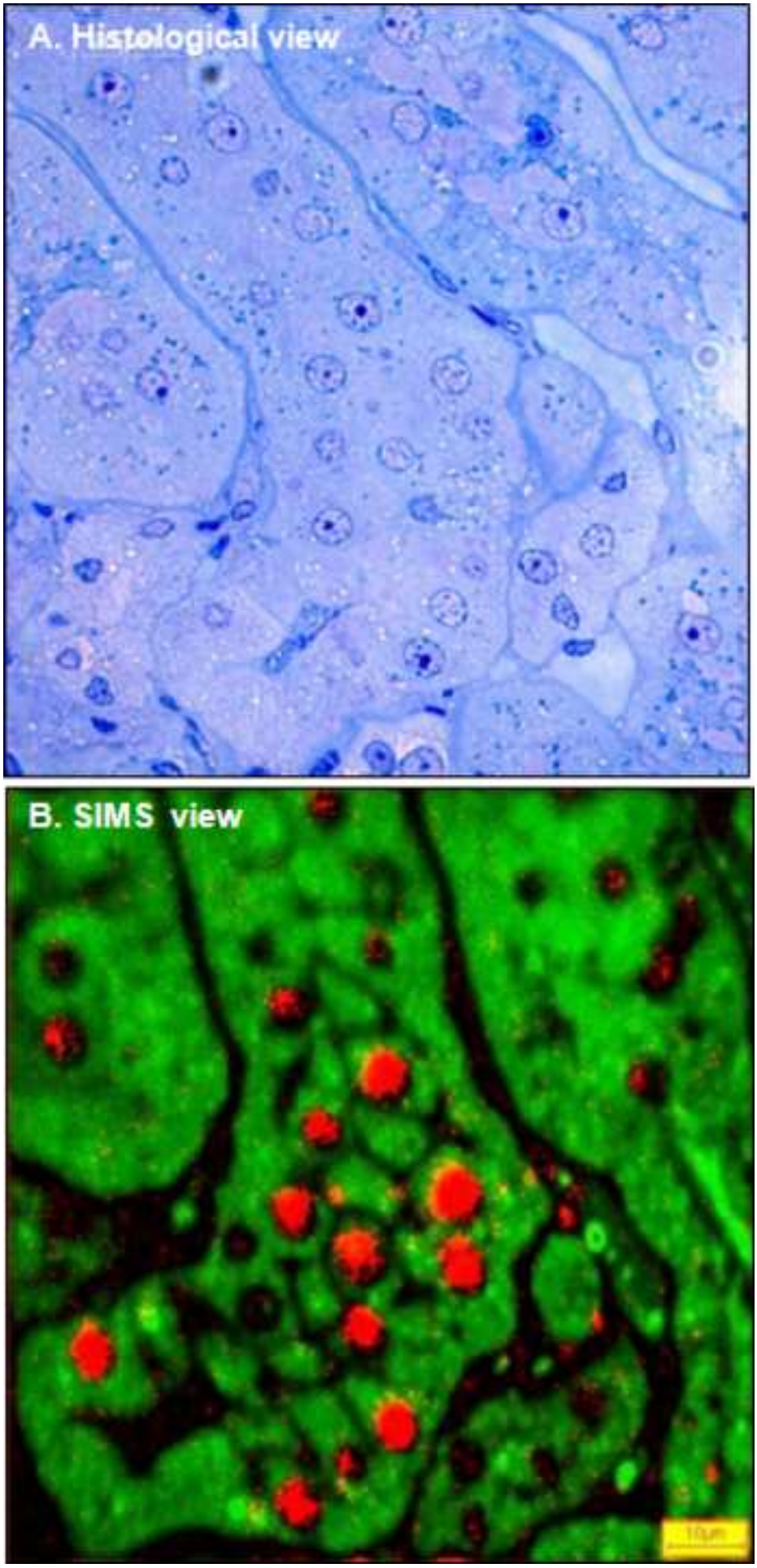

Figure 3

Click here to download high resolution image

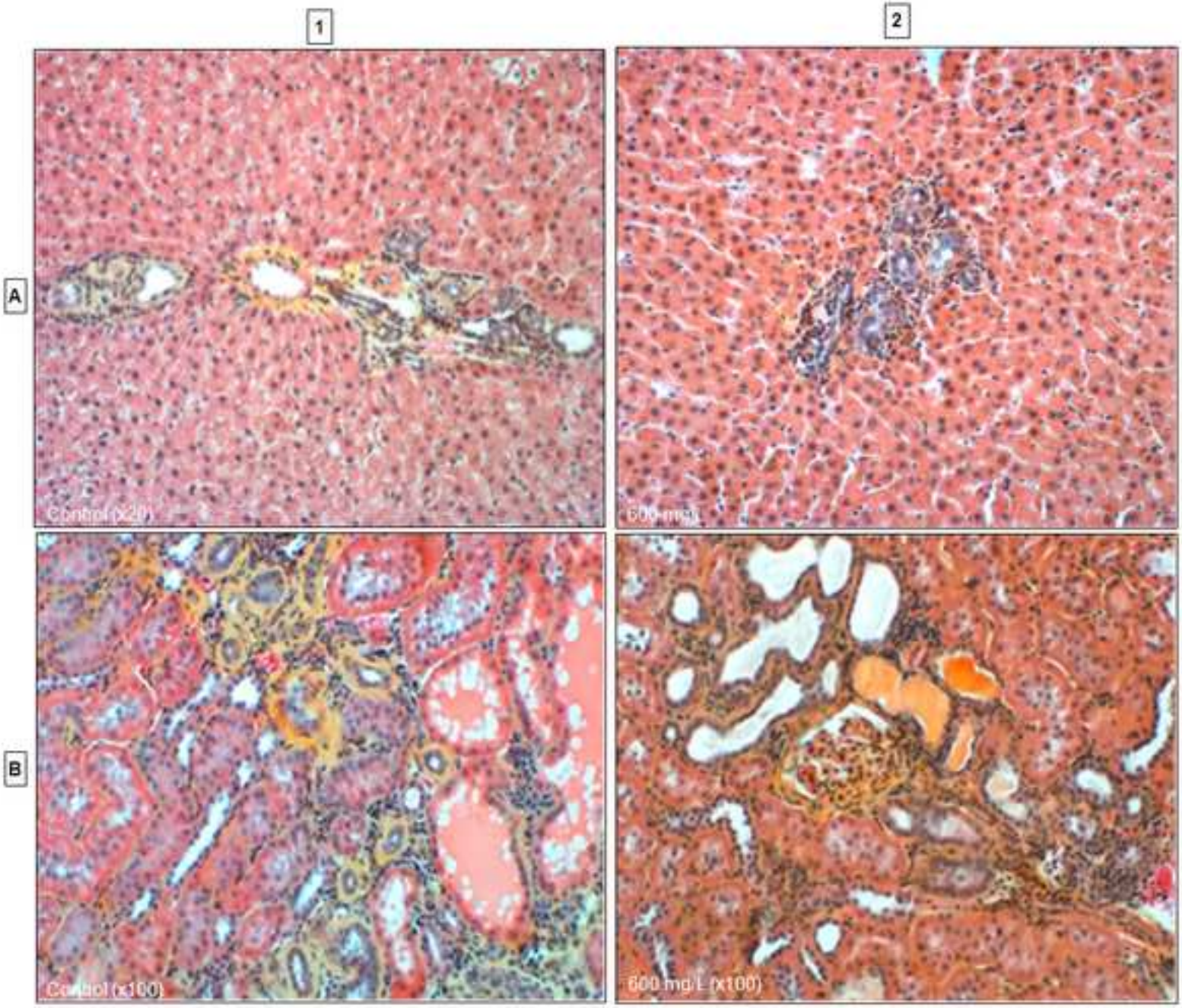

Figure 4

Click here to download Figure: Figure 4 .pptx

Figure 4

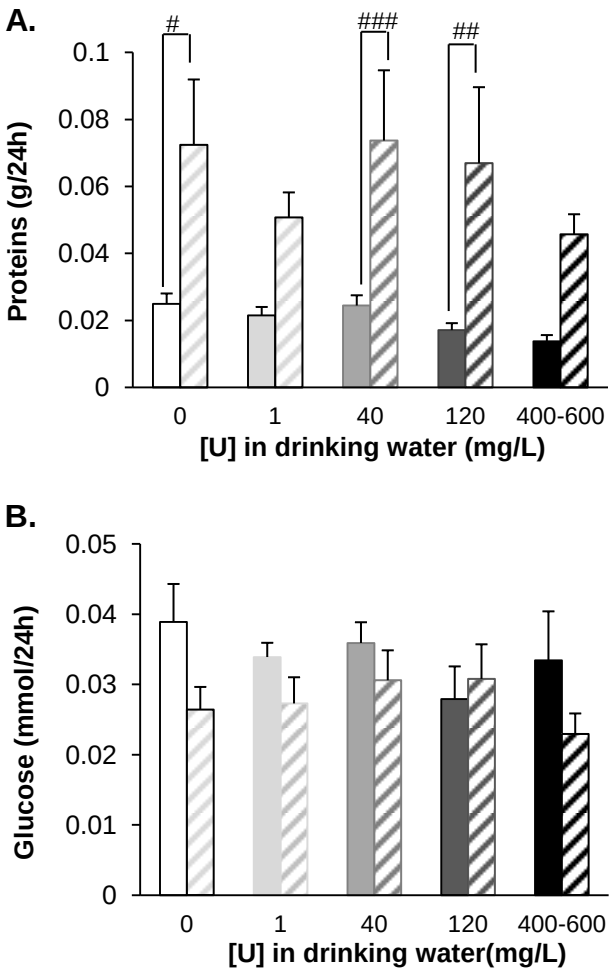

Figure 5

Click here to download Figure: Figure 5 .pptx

Figure 5

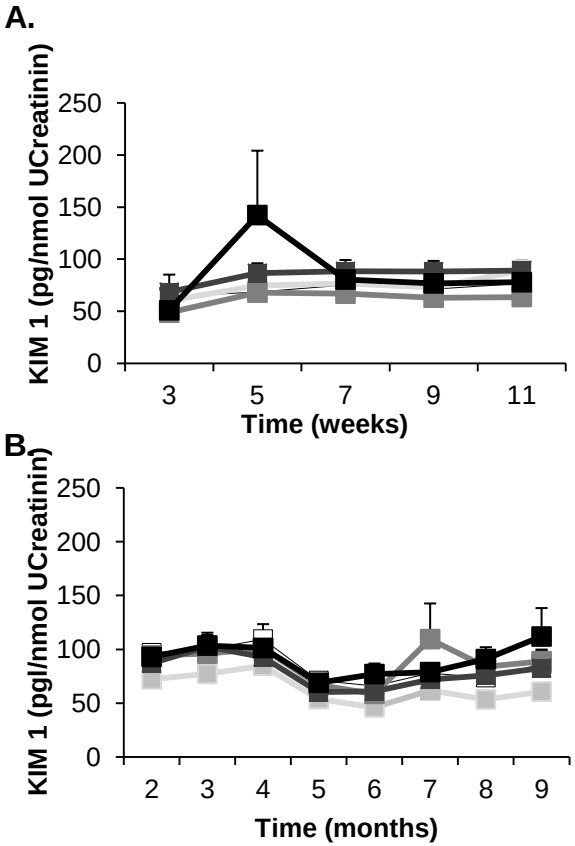

Figure 7

Click here to download Figure: Figure 7.pptx

Figure 7

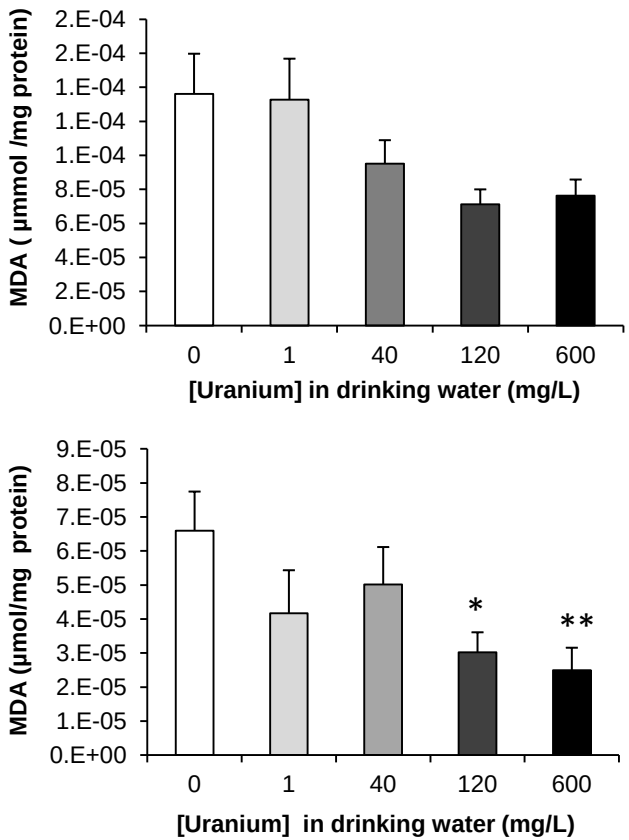

Figure 8

Click here to download Figure: Figure 8 .pptx

Figure 8

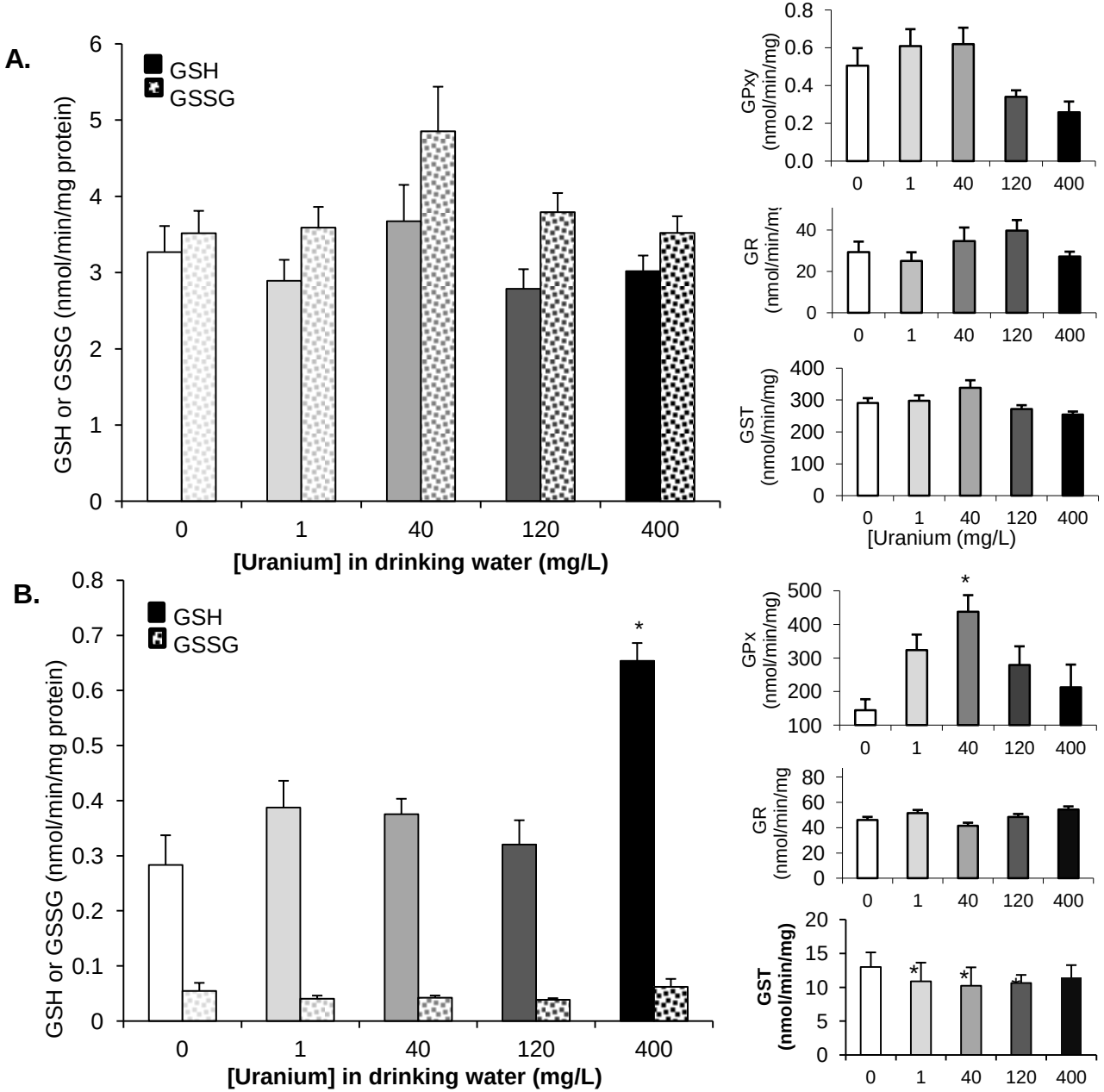

Figure 9

Click here to download Figure: Figure 9.pptx

Figure 9

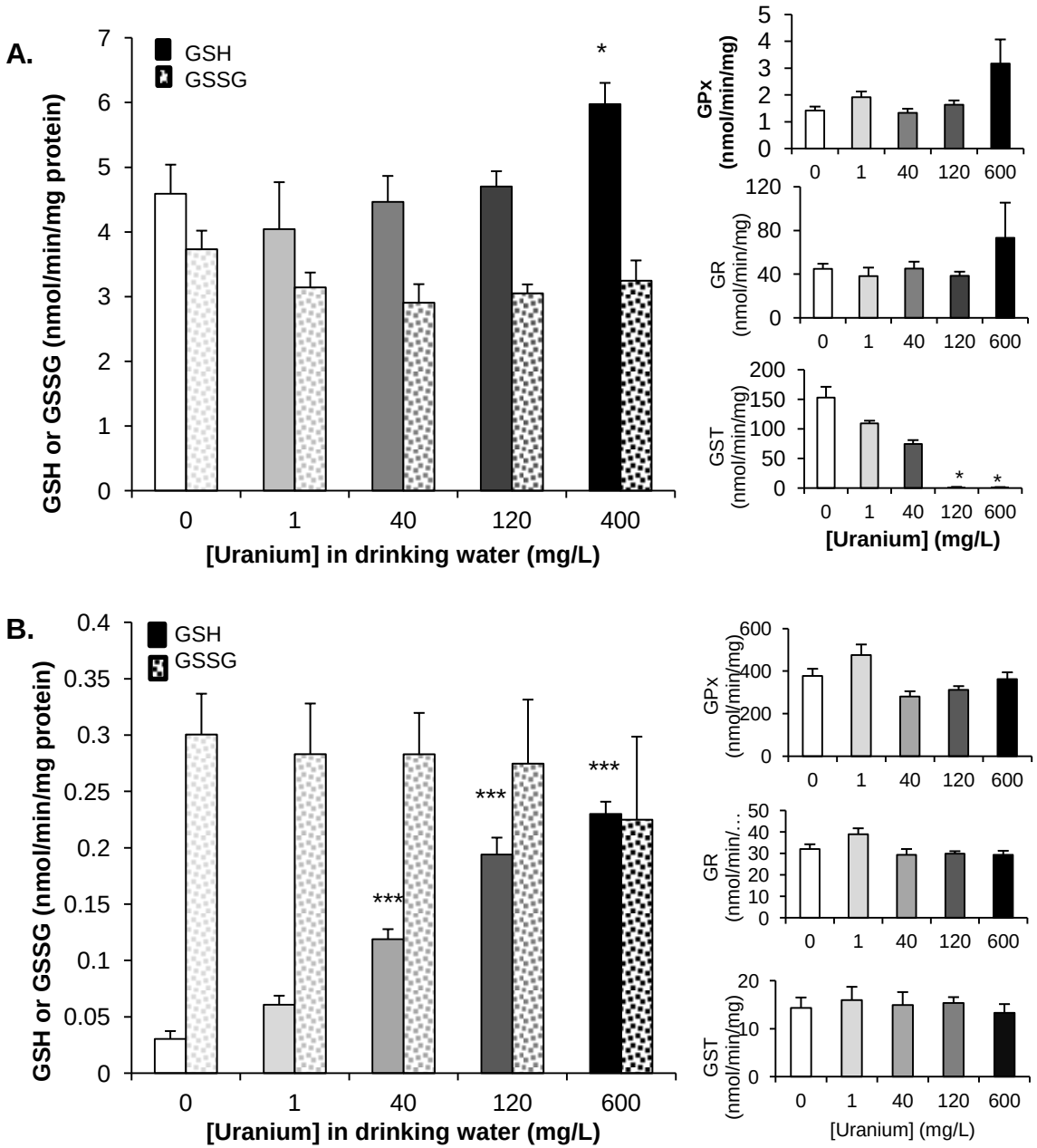

Figure 10

Click here to download Figure: Figure 10.pptx

Figure 10

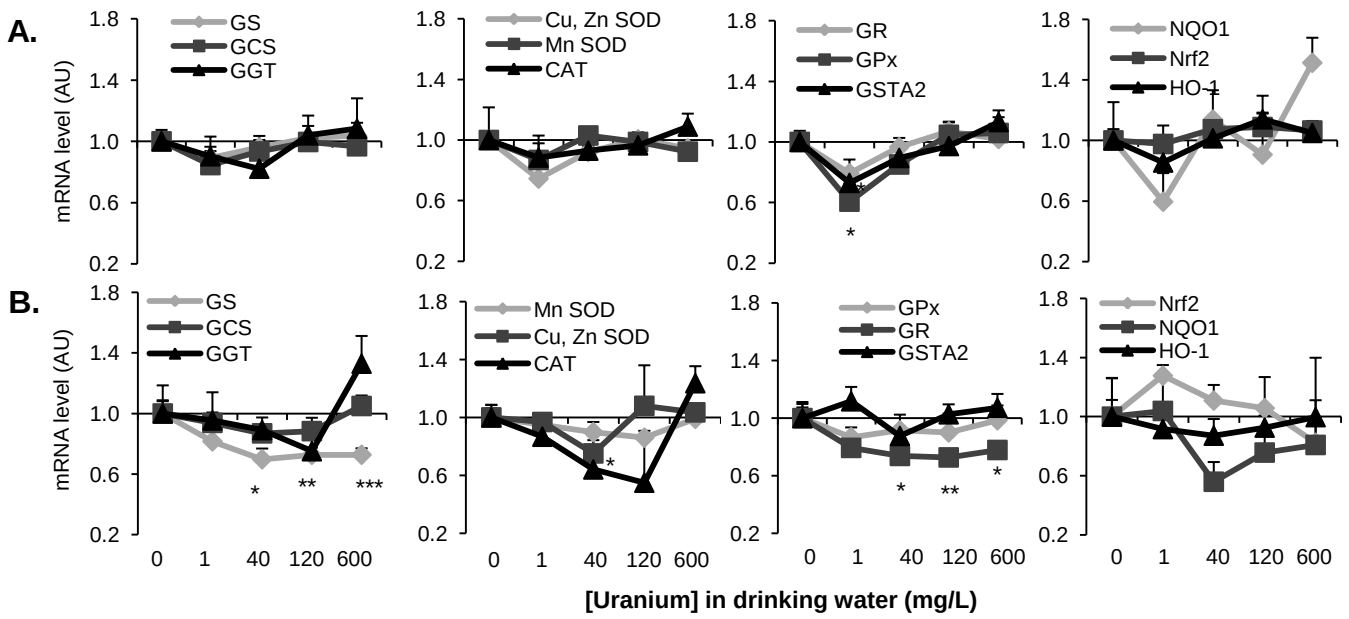

Figure 11

Click here to download Figure: Figure 11 .pptx

Figure 11